Chapter 5
Geochronology of Senèze: $^{40}Ar/^{39}Ar$ Dating and Magnetostratigraphy, with Notes on an ESR/U-Series Dating Attempt

Eric Delson, Sébastien Nomade, Sevket Sen, Evelyne Debard, Jean-François Pastre, Jean-Jacques Bahain, Qingfeng Shao, and Christophe Falguères

Abstract The age of the Senèze mammalian fauna has been discussed since it was first reported in 1892. $^{40}Ar/^{39}Ar$ ages reported by Nomade et al. (2014) and recalculated here to agree with current standards placed the deposits between 2.20 and 2.07 Ma. Paleomagnetic data collected in 2001 and 2004 help to narrow the age range, especially of the levels yielding fossils in 2001–2006. In the western sector, fossils can be securely dated between 2.10 and 2.08 Ma, while in the southeastern sector, they are slightly older, between 2.20 and 2.18 Ma. Senèze is one of the few later Cenozoic European sites dated by both argon geochronometry and paleomagnetism, which makes these ages so precise. Experiments with ESR/U-series dating on teeth proved unsuccessful as a result of the early U-uptake and high natural dose rate in the sediments of Senèze.

Résumé L'âge de la faune mammalienne de Senèze fait débat depuis sa découverte en 1892. Les âges $^{40}Ar/^{39}Ar$ obtenus par (Nomade et al. 2014) sont ici recalculés selon les calibrations les plus récentes et placent définitivement les dépôts de ce site paléontologique majeur entre 2.20 et 2.07 Ma. Les données paléomagnétiques recueillies en 2001 et 2004 permettent d'affiner encore la fourchette d'âge, en particulier pour les niveaux ayant livré des fossiles entre 2001–2006. Dans le secteur occidental, les fossiles peuvent être datés avec une grande précision entre 2.10 et 2.08 Ma, tandis que dans le secteur sud-est, ils sont légèrement plus anciens, entre 2.20 et 2.18 Ma. Senèze est l'un des rares gisements européens du Cénozoique supérieur à être daté à la fois par radio-isotopie et paléomagnétisme, ce qui rend sa datation si précise. Nous notons enfin que les tentatives de datation de dents par ESR/U-Th se sont révélées infructueuses en raison de l'absorption précoce de l'U et du débit de dose naturel élevé des sédiments de Senèze.

Keywords Argon-argon ages • Biochronology • Feni subchron • Huckleberry Ridge excursion • Late Villafranchian • Mammal fauna • MNQ 18 • Paleomagnetism

Mots-clés Ages argon-argon • Biochronologie • Faune mammalienne • Paléomagnétisme • Villafranchien supérieur

E. Delson (✉)
Division of Paleontology, the American Museum of Natural History, New York, NY, USA
e-mail: eric.delson@lehman.cuny.edu

Department of Anthropology, Lehman College of the City University of New York, Bronx, NY, USA

PhD Program in Anthropology, The Graduate Center of the City University of New York, New York, NY, USA

New York Consortium in Evolutionary Primatology, New York, NY, USA

Institut Català de Paleontologia Miquel Crusafont, Barcelona, Spain

S. Nomade
Laboratoire des Sciences du Climat et de l'Environnement, CEA Saclay, 7LSCE/IPSL, UMR CEA-CNRS-UVSQ 8212, Gif sur Yvette, France

S. Sen
CR2P (Paléontologie)—Muséum National d'Histoire Naturelle, 8 Rue Buffon, 75005 Paris, France

E. Debard
Université de Lyon, UCBL, ENSL, CNRS, LGL-TPE, 69622 Villeurbanne, France

J.-F. Pastre
23, rue de l'Eglise, 93370 Montfermeil, France

Laboratoire de Géographie Physique, Environnements quaternaires et actuels, UMR 8591 CNRS, Thiais, France

J.-J. Bahain · C. Falguères
UMR 7194 HNHP, Département Homme et Environnement, Muséum National d'Histoire Naturelle, Paris, France

Q. Shao
College of Geography, Nanjing Normal University, Nanjing, China

E. Delson et al. (eds.), *Senèze: Life in Central France Around Two Million Years Ago*, Vertebrate Paleobiology and Paleoanthropology, https://doi.org/10.1007/978-3-031-64415-3_5

Introduction

The age of the Senèze mammalian fauna has been subject to discussion since it was first reported by Boule (1892). He noted that the proboscidean he recovered was *Elephas meridionalis*, similar to that found in the British Crags, but older than the same taxon at Durfort and Cromer, although younger than the mastodons of Chilhac and Le Coupet. Over the following decades, work by Depéret (1929), Depéret and Mayet (1912), Stehlin (1923), Schaub (1943) and others discussed the fauna as Late Pliocene in age, without suggesting actual dates. Heintz (1970) and Azzaroli (1970) both included Senèze in their Late Villafranchian mammal unit, younger than the Saint-Vallier assemblage, which Guérin thought might date to ca. 2.0–1.9 Ma (Guérin et al. 2004). As summarized in Delson et al. (2006) and Faure et al. (2024), age estimates for the Senèze fauna (not considering the suggestion of Azzaroli et al. (1988) that there was a younger assemblage somehow mixed in) ranged between ca. 1.5 and ca. 2.1 Ma, near the then-accepted Plio-Pleistocene boundary.

Prévot and Dalrymple (1970) provided the first chronometric date for the Senèze complex, a whole-rock potassium-argon date of 2.30 ± 0.15 Ma for samples of the Pié de Charenty lava flow assumed to predate the maar deposits. Couthures and Pastre (1983) and Couthures (1989) reported a roughly comparable date of 2.48 ± 0.06 Ma. All of these works reported a reversed polarity for the flow, correlated to the lower Matuyama. Prévot and Dalrymple (1970) also reported paleomagnetic data for the upper 132.5 m of a core drilled into the lake beds in 1965. The section was entirely reversed, except for a normal zone near the core top, between 17.5 and 23.5 m down from the surface (between 22–23 m and 23.5–28 m, sandy layers did not allow paleomagnetic sampling). This normal interval was correlated to the "Lower Olduvai" which they thought dated ca. 2.1 Ma. Prévot and Dalrymple (1970) estimated that the maar lake filled in about 0.25 Myr (from the 2.35 Malava flow to the 2.1 Ma core top), which agreed with an estimate by Ehrlich (1968) of 200–300 kyr for the age span of the core based on the number of annual diatomite layers in a portion she counted. Delson and Plopsor (1975) discussed these geochronological elements and agreed with Prévot and Dalrymple (1970) that the short normal interval correlated with the Réunion normal magnetosubchron and the Senèze mammalian fauna likely dated between 2.1 and 2.0 Ma, as it was then assumed to derive from levels altitudinally above the lake beds. Roger et al. (2000) reported a $^{40}Ar/^{39}Ar$ age of 2.10 ± 0.01 Ma on a thin tephra within the normal magnetozone near the top of a shorter core, drilled in 1989. They considered that this normal was the Réunion subchron and estimated that the subchron's top would have been close to 2.09 Ma.

Bonnie Blackwell was part of the original Senèze field team and collected a range of data in order to undertake ESR analysis of the age of the site. A preliminary abstract (Mei et al. 2001) reported results from a blind test of the ESR method on teeth which did not in fact come from Senèze. Little further work was done with the Senèze data, in part because it became necessary to include U-series analyses, which was growing more common as time passed. Finally, Blackwell et al. (2020) published another abstract before her untimely death, providing some analytical details: TL dosimetry, γ (gamma) spectrometry and neutron activation analyses measured the sedimentary dosimetry. Sedimentary water concentrations ranged from 11 to 36% by weight. Volumetrically and time-averaged sedimentary and time-averaged cosmic dose rates ranged from 1.5 to 2.0 mGy/yr above and below the Trench 2 layer yielding *Dicerorhinus etruscus* (see below), but up to 3.0–4.0 inside it. For each tooth studied, 5–8 subsamples were independently dated by standard ESR, while U uptake rates were analyzed by isochron analyses. Enamel U concentrations averaged 3–6 ppm, dentine 70–100 ppm, and bone 60–80 ppm depending on the tooth and subsample. Accumulated doses ranged from 2799 to 4721 Grays. Dates for two teeth suggested that bioturbation had mixed younger fauna into the Villafranchian deposits but preliminary dates for *D. etruscus* teeth were 1.5–2.1 Ma, assuming p = 4–8. It is likely, however, that the two teeth which indicated a possibly younger age may have been blind test samples from other localities. Moreover, the subsequent ESR/U-series analyses reported here in the Appendix demonstrated that the assumed value of p (linked to a recent uptake of uranium) was unlikely thus vitiating the date obtained.

Nomade et al. (2014) reported a number of $^{40}Ar/^{39}Ar$ ages from several French Villafranchian faunal sites, including five from Senèze. These tephra derived fron the Mont-Dore stratovolcano (see Pastre 2024). Tephra samples SEN 1 (dated 2.13 ± 0.02 Ma) and SEN 8 (2.17 ± 0.02 Ma) derived from levels below the main faunal horizons in parcel 233 (see below and also Parenti et al. (2024), Debard (2024) and Pastre (2024). SEN 56 (2.09 ± 0.01 Ma) was collected in parcel 234 but is not connected directly to any faunal horizon. SEN 98 (2.21 ± 0.02 Ma) and SEN 101 (2.16 ± 0.02 Ma) were collected in the large trench excavated in parcel 172 and were said to bracket a major fossiliferous level. Details on these samples are presented below, but in brief, one faunal level in parcel 172 appeared to be roughly 2.18 Ma while one in parcel 233 was younger than 2.13 Ma. The overall implication was that Senèze mammals dated between 2.20 and 2.10 Ma. The older Chilhac fauna was dated ca. 2.37 Ma, suggesting that the still older Saint-Vallier assemblage might be at least 2.40 Ma.

Paquette et al. (2021) reported several U–Pb dates on zircon from a number of French Villafranchian sites (see Crégut-Bonnoure et al. 2024), including one of 2.100 ± 0.029 Ma from Senèze. The location given for that sample does not agree with the local geography, but communication with one of the authors (J.-L. Poidevin) revealed that the sample in fact came from our "section A" (see below), which also produced the argon date on sample SEN 56. This level appears to be stratigraphically higher than any recovered fossils.

In addition to collecting tephra samples for argon dating, the team invited Sevket Sen to sample the deposits for evidence of magnetozones at Senèze. The results of this work have not yet been published in detail, although Delson et al. (2006) and Nomade et al. (2014) noted that Sen suggested a short interval of normal polarity occurred high in the section, above the SEN 1 tephra.

In this chapter, Nomade and Delson provide recalculated argon ages based on the most recent standards (Schaen et al. 2021), Delson and Sen interpret paleomagnetic data from five separate sequences, and we place these results into the stratigraphic context provided by Debard (2024). Combining these sources of data, we offer an overall interpretation of the age of the Senèze deposits and faunal horizons. In addition, Bahain, Shao and Falguères discuss (in the Appendix) their unsuccessful attempt to obtain a comparable date using an ESR/U-series approach.

Stratigraphic Context

In order to place the dated samples and paleomagnetic "columns" in the stratigraphic context of Senèze, it is important to briefly consider the positions of the sections yielding the samples and then examine each in detail. Parenti et al. (2024, Fig. 2.3) provide a plan of all the major excavated areas and some additional sections. Our team's work at Senèze can be divided into two main geographic sectors, the western sector with excavations and sections mainly located in cadastral parcels 233 and 234 (these are official land divisions which were passed down through family ownership, see Faure et al. 2024) and the southeastern sector mainly in parcel 172. Because these parcels were used by their owners for pasturage, all excavations and trenches were refilled at the end of each season's work.

In the western sector, trenches 1 and 2 were excavated in 2001 and sampled for magnetostratigraphy and tephra (see Debard 2024, Figs. 3.2 and 3.3 for more detail). Samples SEN 1 and SEN 8 were recovered from trench 2 near the team's first major paleontological find, the partial skeleton of *Dicerorhinus etruscus* (see Guérin 2024). Debard (2024) has described the sediments in these sections (and others nearby) and defined small- and medium-scale units in each, which have been correlated as shown in Table 5.1. The rhino skeleton derived from layer T2hm, and sample SEN 1 was located slightly below it. The upper part of trench 2 (layers T2h–T2j) had slipped downslope so that it now lies at the same altitude as the lower part (layers T2a–T2g), with a small fault between the two parts. Sample SEN 8 derived from one of the stratigraphically lowest levels of this trench (T2b). Note that the tephra samples were extracted from sedimentological samples named S1, S8, etc. on the diagrams. A small cliff face termed section A at the southern end of parcel 234 (near the trailer used as an office) was studied in 2003 and sampled for sedimentology and tephra; sample SEN 56 was recovered near the middle of this section (Debard 2024, Fig. 3.8). The whole of Section A also slipped downslope from its original higher position in the maar, so that this tephra was high in the overall sequence of the site. Also in 2003, an area slightly south of the original trench 2 (termed Zone [H8-N9-L14-G11], hereafter "Zone H8") was excavated. In 2004, a section in Zone H8 was reopened and sampled for magnetostratigraphy (Debard 2024, Fig. 3.6), as was a pit dug for that purpose at the northern edge of parcel 233 (Debard 2024, Fig. 3.7). Thus, three dated tephra and four sets of magnetostratigraphic samples ("columns") derived from the western sector, as summarized in Fig. 5.1. SEN 8 is the stratigraphically lowest (and oldest) sample, followed up-section by several cervid fossils, SEN 1, a partial cervid skeleton, the rhino and other fossils, and then SEN 56 above.

In the southeastern sector, trench 5 was opened in 2004 over a depth of more than 11 m in two segments with a step

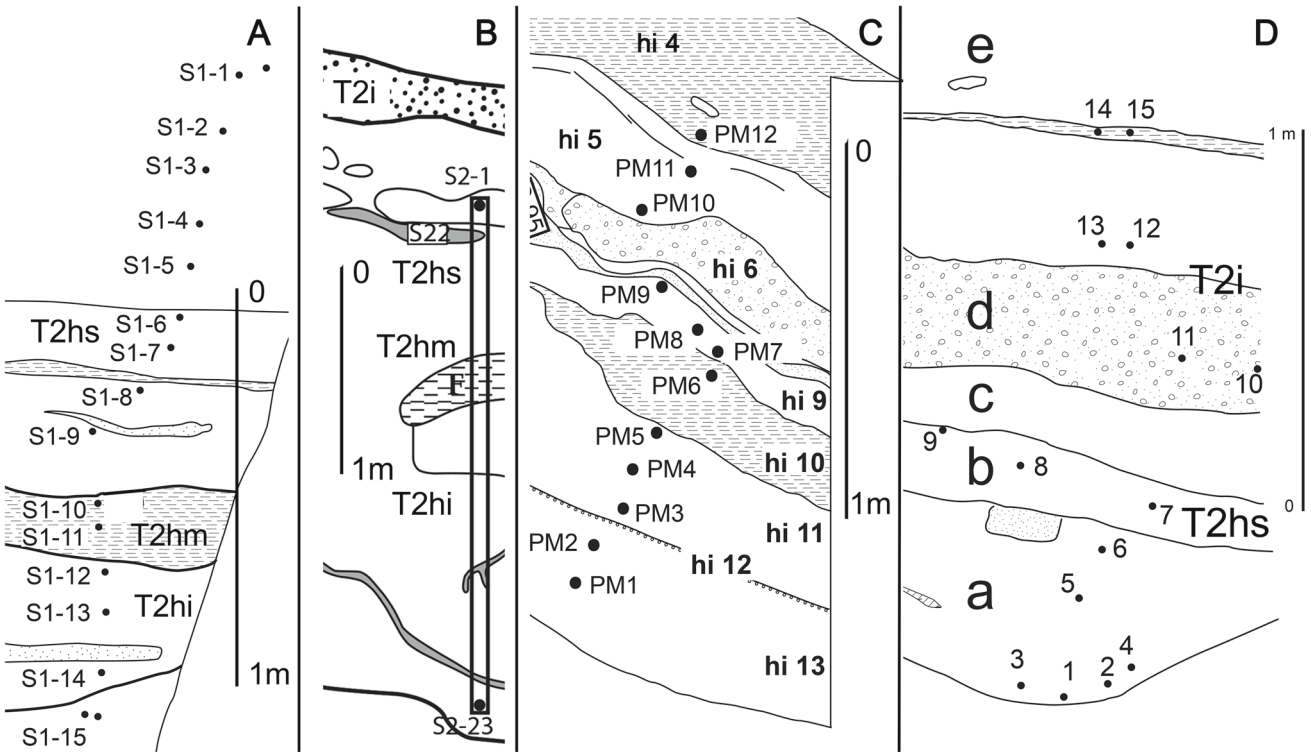

Fig. 5.1 Close-up views of paleomagnetic sampling positions in western sector sections. Scale bars = 1 m. Trench 2 horizon equivalents (T2h, T2i) in A and D approximate, after correlations in Debard (2024). A, Trench 1 (2001), from Debard (2024), Fig. 3.2; paleomagnetic samples S1-1–S1-15. B, Trench 2 (2001), from Debard (2024), Fig. 3.3; T2hm is the sandy level with the *Dicerorhinus* fossil; paleomagnetic samples S2-1–S2-23 shown as a column with intermediate samples not individually labeled; approximate elevation of argon dating sample SEN 1 just above letters "T2hi", although the tephra is actually located about 3 m to the right; sample SEN 8 located below the base of the figure (see Fig. 3.3). C, Zone H8 (2004), from Debard (2024), Fig. 3.6; hi horizons equivalent to those of Trench 2 (T2hi); paleomagnetic samples PM1–PM12. D, Pit at north end of P 233 (2004), from Debard (2024), Fig. 3.7; layers a-c correspond to T2h, while layers d-e correlate with T2i; paleomagnetic samples 1–15 (tabulated as T2-1 through T2-15 in Table 5.4). Note that the SEN 56 tephra is located in section A, not among those shown here; see Fig. 3.8

Table 5.1 Stratigraphic correlations of the western sector (parcels 233 and 234; trenches 1–2 and nearby)

SSet	Trench 1	Trench 2	Zone H8-N9-L14-G11	Pit N P233	Section A
6′	T1i				
5′	T1h	T2j			Upper set
4′	T1g				[U/Pb 2.1 + 0.029][1]
3′	T1f T1e	T2i		d-e [T2i; PM 10–15]	Upper set [SEN 56] (2.07 ± 0.02 Ma)
2′	T1d (PM S1-1–9) T1c (PM S1-10–11) T1b (cervid, PM S1-12–14)	T2hs T2hs (PM S2-1–7) T2hm (fossils, incl rhino; PM S2-8–10) T2hi (SEN 1 T2hi 2, 2.10 ± 0.03 Ma; PM S2-11–23)	[T2]hs [T2]hm [T2]hi (4: PM 12; 5: 10–11 cervid; 9: 7–9; 10: 6; 11: 3–5; 13: 1–2)	b-c [T2hs; PM 7–9] a [T2hs; PM 4–6] a [T2hs; PM 1–3]	Central set
1′	T1a (PM S1-15)	T2g –f [older level in place:] T2e-b (PM S2B-2B-3A) T2b (SEN 8, 2.16 ± 0.05 Ma) T2a (PM S2-B1B)			Lower set

Notes Modified after Debard (2024), Table 3.1; SEN # = argon dated tephra; PM # = paleomagnetic sample numbers; in the column for Zone H8-N8-L14-G11, data for [T2]hi are presented only briefly in the table—for example "4: PM 12" means "sample PM 12 is found in layer hi4", "5: 10-11 cervid" means "samples PM 10 and 11 and cervid fossils are found in layer hi5"

[1]Zircon date on unknown level of Section A from Paquette et al. (2021).

in between, total length ca 25 m. Sets of paleomagnetic samples were taken in each segment, and tephra samples SEN 98 and SEN 101 were collected, although due to a numbering change, these tephra samples do not correspond to sedimentological samples S98 and S101 (Fig. 5.2; see Debard 2024, Figs. 3.11 and 3.12 for more detail). In 2005, an area equivalent to lower trench 5 was reopened as trench 6, and the greater part of an equid skeleton was recovered (see Eisenmann and Delson 2024). Another partial equid skeleton was found in 2006 in the nearby trench 7. Correlations among the samples and equids is complex, but there is clear overlap between the two argon-dated samples and the magnetostratigraphic "columns". Table 5.2 is an attempt to show such correlations. Broadly, the 2005 *Allohippus* skeleton was found in layer 1.2, near the base of the sequence, followed upsection by additional fossils including two partial cervid crania recovered in 2004 and the 2006 *Allohippus* skeleton, with the SEN 98 and SEN 101 tephra above these.

Following Debard (2024), no direct correlation is possible between the two sectors, but the argon dating results reveal broad similarity in age.

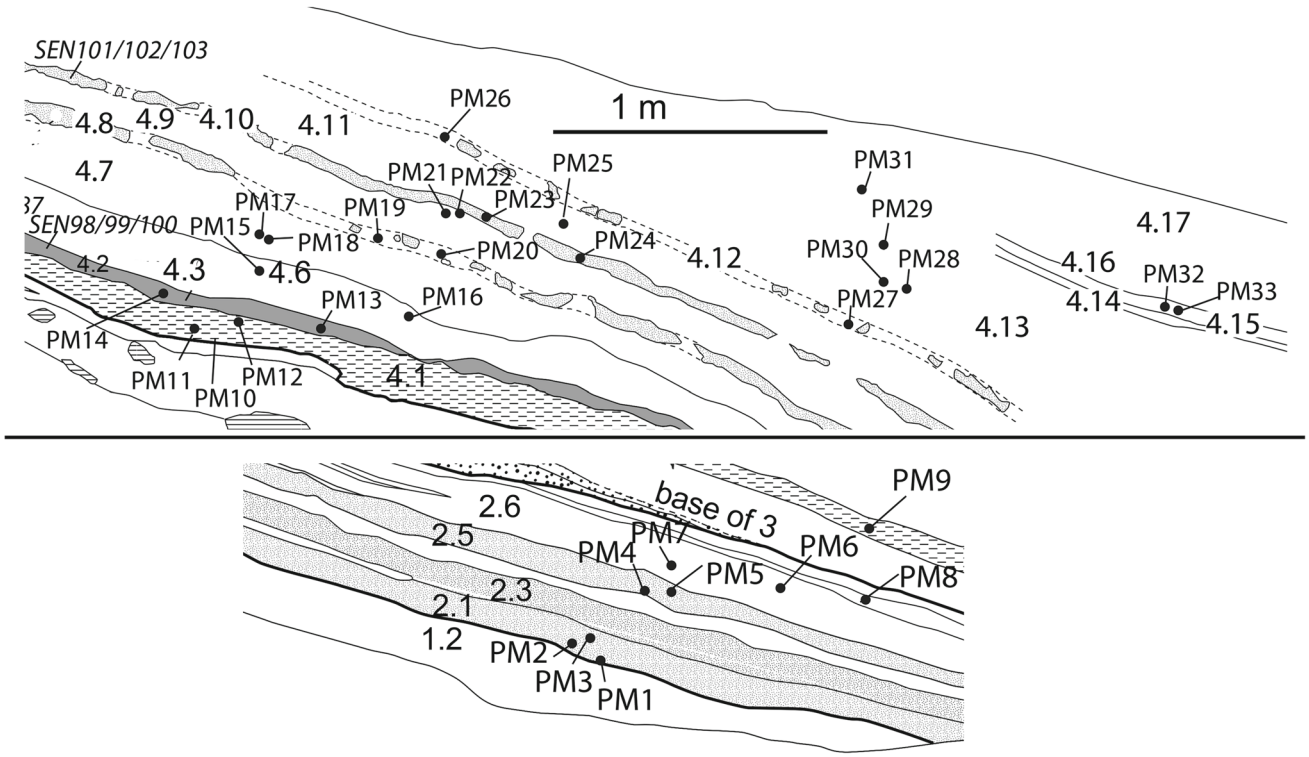

Fig. 5.2 Close-up views of paleomagnetic sampling positions in southeastern sector Trench 5. Above, Trench 5 lower part (inf) with layers 4.1–4.17 and paleomagnetic samples PM10-PM33; the positions of tephra samples SEN 98 and SEN 101 (each as part of a group of nearby samples) are shown at left. Below, Trench 5 upper (sup, stratigraphically below T5 inf), with layers 1.2–3 and paleomagnetic samples PM1-PM9. The 1 m scale bar is accurate for both parts

Table 5.2 Stratigraphic correlations of the southeastern sector (parcel 172; trenches 5–7)

Set	Trench 5 sup	Trench 5 inf	Trench 6	Trench 7 sup	Trench 7 inf
6					
5 (slope)			5 (gravels on erosional surface)		5 (slope, slippage at base?)
4 (lacustrine with some slope)		4.16–4.1	4.20–4.7	("step" between T7 sup & inf)	4.20–4.8
		(PM T5 10–31 in 4.13–4.1)		4.13, 4.12, 4.9	
		(4.10 SEN 101, 2.13 ± 0.04 Ma)		(downslope part only)	
		(4.2 SEN 98, 2.18 ± 0.03 Ma)		4.8–4.1	
		(set 4 visible and overlies set 1 in downslope part only)		(set 4 overlies set 1)	
3 (slope)	3	3		3	
	(PM T5 1–9)			(antlers in conglomerate)	
	Fossils at base			(*Allohippus* skeleton 2006)	
2 (slope)	2.6–2.1	2.6–2.5		2b (fossils) Lake shore	
		2.4 (fossils)			
		2.3–2.1		2a	
1 (slope)		1.3–1.4		1b	
		1.2			
		(*Allohippus* skeleton 2005)		1a	
		1			

Notes SEN # = argon dated tephra; PM # = paleomagnetic sample numbers

$^{40}Ar/^{39}Ar$ Dating

Samples SEN 1, SEN 8, SEN 56, SEN 98 and SEN 101 were analyzed at the $^{40}Ar/^{39}Ar$ facility hosted at the LSCE (Gif-sur-Yvette, France). In order to check the accuracy of these measurements and test possible inter-laboratory bias, SEN 1 was also analyzed at the Berkeley Geochronology Center (USA). In both laboratories, pristine sanidine crystals ranging from 160 to 400°m in size were handpicked from a K-feldspars concentration and slightly leached for 5 min in a 5% HF acid solution. A total of 25–40 grains for each sample were loaded in aluminum disks along with standard reference minerals and irradiated in a nuclear reactor. All basic data from both labs were reported in Supplementary online Tables T1 and T2 of Nomade et al. (2014) and are not repeated here.

Gif sur Yvette Laboratory Analytical Method

Samples were irradiated for 90 (Irr. 1b, SEN 1, SEN 8 and SEN 56) and 60 min (Irr. 20, SEN 98 and SEN 101) in the B1 tube of the OSIRIS reactor (CEA Saclay, France). After irradiation, samples were transferred to a stainless steel sample holder and then into a differential vacuum Cleartran© hublot. Single grains were fused (with 9% of the laser power) using a focused 25 W CO_2 laser (Synrad©). Ar isotopes were analyzed using a micromass 5400 mass spectrometer equipped with a single ion counter (Balzers© SEV 217 SEN). Depending on the xenocrystic contamination, 7 to 15 sanidine single crystals were individually dated for each sample. Neutron fluence (J) was monitored by co-irradiation of Alder Creek Sanidine (ACs-2, Nomade et al. 2005) or Fish Canyon Sanidine (FCs, Renne et al. 1998) placed in the same pit as the sample or in three positions around the sample. The J value for each sample was determined from fusion analyses of 3–6 ACs-2 or FCs single grains. Corresponding J values were calculated using an age of 1.193 Ma (Nomade et al. 2005) and 28.02 Ma (Renne et al. 1998) for ACs-2 and FCs respectively, as well as the total decay constant of Steiger and Jäger (1977). J uncertainty is calculated using the standard deviation of all measurements and excludes age uncertainty on the standard age as well as the decay constant. Procedural blanks were measured every two or three grains depending on the unknown bean size previously measured. For example with a 9 min static blank, typical backgrounds are about 2.0×10^{-17} and 5.0×10^{-19} mol for ^{40}Ar and ^{36}Ar, respectively. Each Ar isotope measurement consists of 20 cycles by magnetic switching of the argon spectrum and baselines. The precision and accuracy of the mass discrimination correction was monitored by periodic measurements of air argon. This monitoring is performed using a dedicated air calibration system featuring a 6 l tank filled with purified atmospheric argon. This tank is connected to the mass

spectrometer through the laser extraction system via two pneumatically-actuated air pipettes of approximately 0.1 and 1.0 cc. This system allows for 1 cc (e.g., ~600,000 counts/second [cps] on ^{40}Ar) and 0.1 cc (e.g., ~70,000 cps on ^{40}Ar) atmospheric aliquots to be delivered into the mass spectrometer and permits a careful monitoring of the mass discrimination over a wide dynamic range with a precision better than 0.2% (2σ)for any given bean size measured (see Nomade et al. 2010 for more details). This level of precision allows the user (in theory) to measure with confidence samples with <1% ^{40}Ar* (* indicates radiogenic argon). As the measurements were done during two periods in 2008 and 2010, two discrimination calibration curves (see Nomade et al. 2010 for a calibration curve) were used to correct measurements.

Berkeley Geochronology Center Analytical Method

The SEN 1 aliquot was irradiated for 30 min in the CLICIT facility of the TRIGA reactor at Oregon State University. After irradiation, 34 single grains of sanidine were fused with a defocused argon laser (Synrad) then analyzed with a MAP 215C mass spectrometer at the Berkeley Geochronology Center using methods described by Renne et al. (1998). Procedural blanks were measured between every three grains, and typical values were $3.3 \pm 0.5 \times 10^{-16}$ for ^{40}Ar and $2.26 \pm 0.3 \times 10^{-18}$ for ^{36}Ar moles. Neutron fluence (J) was monitored by Alder Creek sanidine (ACs-2, 1.193 Ma, Nomade et al. 2005) grains in four positions in the Al disk. The J value for each disk was determined from individual analyses of 6 separate ACs-2 crystals in each position fused with the CO_2 laser (total of 24 grains) per disk. The corresponding J values and associated uncertainties were calculated with the total decay constant of Steiger and Jäger (1977) and exclude age uncertainties on the ACs-2 age and the decay constant. Mass discrimination was monitored by automated analysis air pipettes, interspersed with the unknowns.

Recalculation of Ages

Since the dates were published (Nomade et al. 2014), revised calibrations were recommended by the Ar/Ar community for the ACs-2 flux standard (Jicha et al. 2016; Niespolo et al. 2017; Schaen et al. 2021) as well as the decay constant (Min et al. 2000; Renne et al. 2011). Overall these new calibrations insure a better accuracy for the ^{40}Ar/^{39}Ar ages. The use of these new calibrations affects the weighted mean age calculations made previously by <1%, therefore well within the uncertainties reported at the time. However, and to comply with these new recommendations, hereafter all weighted mean ages are recalculated according to ACs-2 at 1.1851 Ma (Schaen et al. 2021) and using the K total decay constant proposed by Min et al. (2000). The recommended revised age for FCs is 28.21 Ma, indistinguishable from the value used in several runs at Gif, and thus these dates are not modified.

^{40}Ar/^{39}Ar Results

Full analytical details for individual crystal experiments corrected for backgrounds and radioactive decay were reported in Supplementary online Tables T1 and T2 of Nomade et al. (2014). Age-probability density spectra with individual single crystal age (2 σ) for each ash layer are presented in Fig. 5.3. Detailed results for each tephra layer are discussed below and summarized in Table 5.3. Uncertainties are reported below at the 2 σ level (corresponding to a 95% probability of accuracy) including J value uncertainties and the K decay constant.

Table 5.3 Summary of ^{40}Ar/^{39}Ar dated samples from Senèze

Sample	Lab	n/N	Age[a] (weighted mean) (ka)	Error (2 s) internal (ka)	Error (2 s) external (ka)	MSWD	Isochron age[a] (ka)	Error (2 s) (ka)	^{40}Ar/^{36}Ar in	Error (2 s)	MSWD	"Best age" (Ma)	Error (2 s) (Ma)
SEN 1	GIF (France)	5//7	2119	24	49	1.0	2080	76	310	23	0.8	N/A	
SEN 1	BGC (USA)	18//34	2100	13	26	0.5	2100	31	316	42	0.5	N/A	
SEN 1 combined		27//41	2110	13	26	1.0						2.10	0.03
SEN 8	GIF (France)	15//15	2159	22	45	1.7	2163	45	291	4	1.2	2.16	0.05
SEN 56	GIF (France)	10//10	2066	9	21	1.4	2074	21	292	8	0.8	2.07	0.02
SEN 98	GIF (France)	9//9	2177	16	32	1.0	2177	33	296	9	1.2	2.18	0.03
SEN 101	GIF (France)	9//12	2133	14	42	0.5	2130	44	311	24	0.3	2.13	0.04

Notes [a]Ages recalculated according to ACs-2 at 1.1851 Ma (Schaen et al. 2021) and K decay constant from Min et al. (2000)
Basic data were reported in Supplementary online Tables T1 and T2 of Nomade et al. (2014)
n/N = number of grains used to calculate age/total number of grains analyzed. MSWD = Mean Square Weighted Deviation

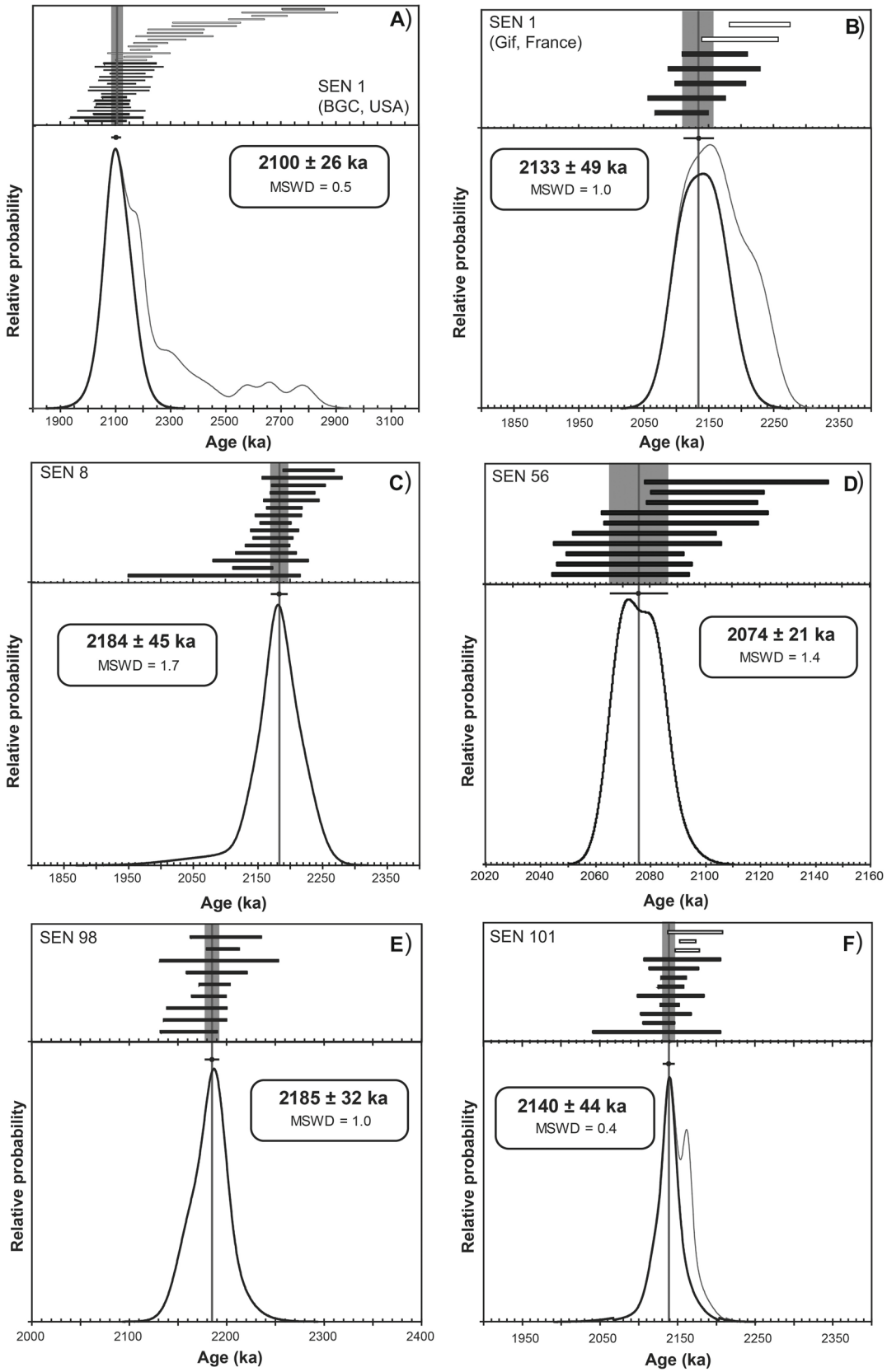

Fig. 5.3 Age probability diagrams of the $^{40}Ar/^{39}Ar$ experiments on Senèze tephra. Black boxes are juvenile crystals whereas white ones correspond to xenocrystals and were not used for the age calculation. Full external uncertainties (1 sigma) are indicated for each weighted mean and isochron ages. A and B indicate results for the US and French analyses on SEN 1, respectively. The dates shown were not recalculated, but those in the text and Table 5.3 were

SEN 1. A total of 7 and 34 sanidine crystals were individually analyzed at Gif and the BGC, respectively, for this ash layer. The corresponding probability spectra are complex with a strong asymmetry toward older ages (Fig. 5.3A, B). This complex distribution can be due to partial incorporation of extraneous argon and/or the presence of xenocrysts from older eruptive events incorporated during the explosive phase. Despite this complex behavior, probability spectra display a dominant mode including the majority of the analyzed sanidine allowing the calculation of robust eruptive ages of 2.10 ± 0.03 Ma (n = 18/34) and 2.12 ± 0.05 Ma (n = 5/7) for the Berkeley and Gif experiments, respectively. Because all crystals analyzed belong to the same tephra layer, a mean age of 2.11 ± 0.03 Ma (n = 27/41) is calculated by combining all single crystal ages. Because of the relatively low spread for each laboratory, the calculated $^{40}Ar/^{36}Ar$ initial ratios have large uncertainties and values above 310 (ca. 310 ± 23 and 316 ± 42) but suggest within error an atmospheric ratio (Table 5.3).

SEN 8. Fifteen sanidine crystals were analyzed for this ash layer. The age probability spectrum exhibits a unimodal pattern leading to a robust eruptive age of 2.16 ± 0.05 Ma (n = 15/15) with a MSWD of 1.7 (Fig. 5.3C) for this tephra layer. The inverse isochron yields a precise initial $^{40}Ar/^{36}Ar$ ratio. The age calculated from this isochron is 2.16 ± 0.05 Ma (MSWD = 1.2), identical to the weighted mean age calculated using all the single crystal ages.

SEN 56. Ten sanidine crystals extracted from this tephra layer were dated, and all of them share the same age within uncertainties, resulting in an almost Gaussian probability diagram allowing us to calculate a robust weighted mean age of 2.07 ± 0.02 Ma (MSWD = 1.4, n = 10/10) (Fig. 5.3D). The corresponding inverse isochron displays a relatively low spread but allows calculation of an age of 2.07 ± 0.02 Ma (MSWD = 0.8) and an atmospheric initial $^{40}Ar/^{36}Ar$ intercept of 292 ± 8.

SEN 98. Nine crystals were analyzed for this tephra horizon. The sanidine population probability spectrum exhibits a simple almost Gaussian distribution allowing calculation of a straightforward mean age of 2.18 ± 0.03 Ma including all analyzed single crystals (n = 9/9) (MSWD = 1) (Fig. 5.3E). The corresponding inverse isochron calculated with this sanidine population displays a nice spread with an initial $^{40}Ar/^{36}Ar$ ratio of 296 ± 9, identical with an atmospheric ratio. The age of 2.18 ± 0.03 Ma (MSWD = 1.2) is identical to the weighted mean age calculated using all the single crystal ages.

SEN 101. Twelve sanidine crystals were analyzed. The probability spectra obtained is here bimodal with a main mode corresponding to 9 crystals. The secondary older peak is probably the result of contamination by older xenocrysts. The main mode allows us to calculate a weighted mean age of 2.13 ± 0.04 Ma (n = 9/12) with a MSWD of 0.5 (Fig. 5.3F). The corresponding inverse isochron displays an initial $^{40}Ar/^{36}Ar$ ratio of 311 ± 24, identical within error to the atmospheric ratio. The age calculated from this isochron is 2.13 ± 0.04 Ma (MSWD = 0.3), in agreement with the weighted mean age calculated using the primary crystal population.

Magnetostratigraphic Analysis

Magnetostratigraphic Sampling

In 2001, S. Sen sampled trenches 1 and 2 for paleomagnetic analysis. The apparently older Jeune Pireyre volcanoclastic deposit was also sampled, but these deposits are unrelated to the mammalian fossils and entirely reversed, so they are not further discussed here. All samples were drilled and the cores cut in the laboratory to obtain cylindrical blocks of standard volume: diameter 25 mm, height 22 mm. Analyses were performed by S.S. in the Laboratoire de Paléomagnetisme of IPG, Paris, using a three-axis 2G cryogenic magnetometer. Bulk susceptibility was measured at room temperature, and samples were thermally demagnetized from room temperature (20 °C) to 350 or 400 °C in 50° increments; a selection of orthogonal projection (Zijderveld) diagrams for 9 samples from the upper part of the Trench 2 section are presented in Fig. 5.4. Fourteen samples were analyzed from trench 1, and a soft secondary component of magnetization was removed before 250 °C, after which there is a stable component. Twenty-two samples were analyzed from trench 2, with a soft component removed by 200° C. Three additional samples were taken in the block which enclosed dating sample SEN 8. Basic data are provided in Table 5.4, and positions of samples are shown above in Fig. 5.1.

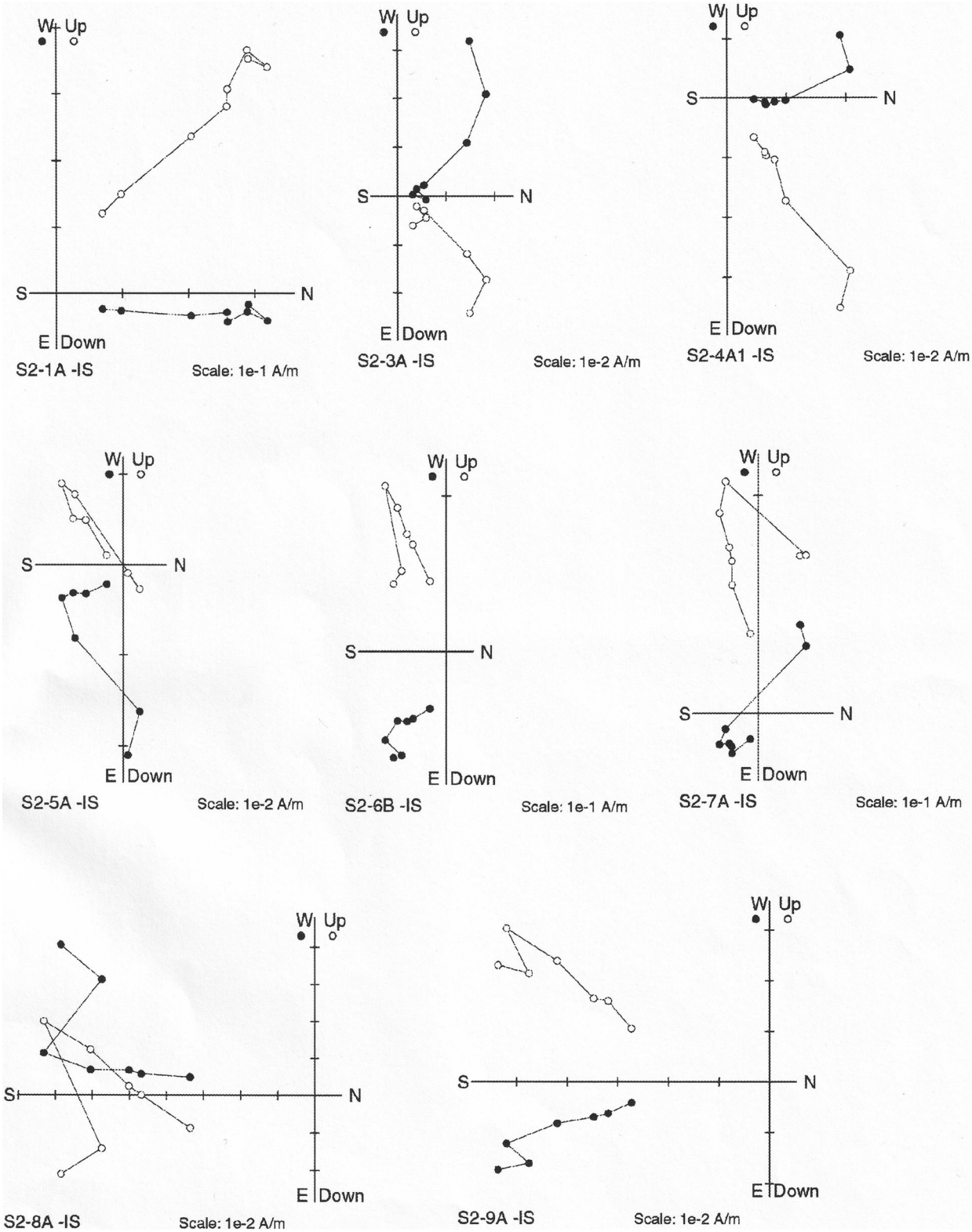

Fig. 5.4 Orthogonal projection (Zijderveld) diagrams for 9 samples from the upper part of the Trench 2 section; see Fig. 5.1B, vertical column headed S2-1. Solid data points are vector end points projected onto the horizontal plane (declination), and open data points are vector end points projected onto a north–south oriented vertical plane (inclination). Thermal demagnetization proceeded from 20° C (room temperature) to 50° and thence to 350° or 400° in 50° steps

Table 5.4 Data for paleomagnetic samples from Senèze "sections"

Location	Sample no.	Height in cm	Declination	Inclination	VGP lat	Polarity
Trench 1	S1-15A	154	172	−61	−83.5	R
(2001)	S1-14A	143	180	−22	−56.4	R
Parcel 234	S1-13A2	128	200	−20	−51.3	R
	S1-12B	115	178	−30	−61.1	R
	S1-11A	107	200	−47	−66.9	R
	S1-10A	100	158	−36	−59.1	R
	S1-9A	83	152	−53	−65.7	R
	S1-8A	72	190	−62	−82.6	R
	S1-7A	65	175	−60	−84.5	R
	S1-6A	57	202	−40	−61.4	R
	S1-5A	47	185	−34	−63.3	R
	S1-4B	37	245	−20	−24.9	R
	S1-2A	15	330	−32	−21.9	R
	S1-1B	0	152	−35	−55.4	R
Trench 2	S2-1A	240	7	−49	14.8	N
(2001)	S2-3A	210	338	30	55.7	N
Parcel 233	S2-4A	199	7	54	78.2	N
	S2-5A	194	150	−45	−59.8	R
	S2-6B	182	120	−57	−45.4	R
	S2-7A	176	140	−76	−61	R
	S2-8A	165	187	−14	−51.6	R
	S2-9A	160	169	−29	−59.1	R
	S2-10A	153	172	−45	−70.5	R
	S2-11A	138	148	−8	−40.4	R
	S2-12A	126	155	−35	−57	R
	S2-13A	117	75	−50	−11.8	R
	S2-14A	108	185	-43	−69.6	R
	S2-15A	96	160	−39	−61.8	R
	S2-16A	84	150	−50	−62.6	R
	S2-17A	73	180	−50	−75.8	R
	S2-18A	61	182	−53	−78.5	R
	S2-19A	49	185	−61	−85.3	R
	S2-20A	41	195	−49	−70.8	R
	S2-21A	29	175	−52	−77	R
	S2-22A	10	181	−57	−82.6	R
	S2-23A	0	151	−47	−61.5	R
Trench 2						
Below fault	S2-B3A	33	175.7	−73.1	−76.2	R
	S2-B2B	12	181	−57.5	−82.9	R
	S2-B1B	0	153.7	−41.4	−59.8	R
Zone H8	P12	140	145	−30	−49.4	R
(2004)	P11 B	125	180	−50	−75.8	R
Parcel 233	P10 A	115	175	−50	−75.3	R
	P9	95	175	−42	−68.8	R
	P8	89	175	−60	−84.5	R
	P7	77	175	−40	−67.4	R
	P6	71	155	−15	−46.8	R
	P5	51	160	−40	−62.4	R
	P4	36	155	−38	−58.7	R
	P3	24	170	−52	−75.4	R
	P2	12	170	−50	−73.8	R
	P1	0	170	−45	−69.9	R
Pit N P233	T2-15	149	100	−45	−25.2	R
(2004)	T2-14	149	215	18	−27.3	R

(continued)

Table 5.4 (continued)

Location	Sample no.	Height in cm	Declination	Inclination	VGP lat	Polarity
Parcel 233	T2-13	124	165	−60	−78.3	R
	T2-12	124	140	−45	−53.2	R
	T2-11	94	260	−10	−10.6	R
	T2-10	91	263	8	−2.1	R
	T2-9	71	340	69	74.9	N
	T2-8	59	190	−50	−73.8	Trans?
	T2-7	49	0	70	81.1	N
	T2-6	34	340	70	74.3	N
	T2-5	24	350	65	82.8	N
	T2-4	14	320	36	48.6	N
	T2-3	7	188	−39	−66.1	R
	T2-2	4	189	−57	−80	R
	T2-1	0	195	−62	−79.1	R
Trench 5	T5-31	250	184.1	−70.2	−80.4	R
Lower/inf	T5-30	250	60.2	−51.0	−4.2	R
(2004)	T5-29	237	29.3	−30.8	22.9	N
Parcel 172	T5-28	222	105.2	−60	37.1	N
	T5-27	202	87.1	−35.8	−11.9	Trans?
	T5-26A	202	97.2	−52	−27.1	Trans?
	T5-25	192	75.2	−30.2	−1.5	Trans?
	T5-24B	180	64.2	−15.8	11.7	Trans?
	T5-23	178	75.3	−15.4	5.8	Trans?
	T5-22	174	205.3	−25.4	−51.5	R
	T5-21	174	167.5	−17.5	−52.1	R
	T5-20	160	50.00	−64.3	−11.5	Trans?
	T5-19	155	89.60	46.8	19.8	Trans?
	T5-18	145	112.3	−8.60	−18.6	Trans?
	T5-17	145	105.0	3.50	−9.2	Trans?
	T5-16	130	89.40	−60.0	−27.4	R
	T5-15	130	126.0	−58.1	−50.1	R
	T5-13	113	212.2	−71.2	−67.3	R
	T5-12	105	146.2	−55.6	−63	R
	T5-11	105	130.4	−53.2	−50.7	R
	T5-10A	97	169.3	−55.7	−77.9	R
Trench 5	T5-9	77	190.9	−23.2	−55.5	R
Upper/sup	T5-8	47	207.6	−48.9	−63.4	R
(2004)	T5-7	41	196.7	−36.1	−61.2	R
Parcel 172	T5-5	28	187.0	−65.2	−84.8	R
	T5-4B	24	167.0	−41.2	−65.9	R
	T5-3	17	117.2	−55.3	−42.4	R
	T5-2	5	182.3	−60.6	−85.9	R
	T5-1	0	190.4	−70.3	−78.7	R

Notes Height in cm above base of sampled sequence; VGP lat., virtual geomagnetic pole latitude; Polarity, estimated from VGP lat.: R, reversed; N, normal; trans?, possibly transitional

In 2004, S.S. sampled three more areas. Twelve samples were collected in Zone H8 and 15 in the pit dug for this purpose at the north edge of parcel 233 (see Fig. 5.1). In trench 5, nine samples were collected in the upper portion (T5 sup), but one was discarded; 24 were collected in the lower portion (T5 inf), but three were lost. As a result of slippage of the upper layers, T5 inf is in fact stratigraphically higher than T5 sup. Dated tephra SEN 98 and SEN 101 were collected in horizons that had been sampled for paleomag (see Fig. 5.2). Samples were thermally demagnetized from 20 °C up to 650 °C, with increments of 50° after the 150° step. These samples were found to have no reliable secondary magnetization or just a very soft one that is removed before the 200 °C step. Thereafter, a stable component was defined in all samples with a very low angle error. Some samples showed an unstable viscous magnetization behavior after the 500 °C step, when the direction became random. In such samples, the results at steps over 500° were discarded. Basic data are provided in Table 5.4.

Magnetostratigraphic Results

In parcels 233 and 234, four separate but correlated "sections" yielded paleomagnetic signal (Fig. 5.5). Three magnetozones can be distinguished. A reversed zone is recorded in the two upper layers (d and e) of the pit at the northern edge of parcel 233 (Fig. 5.5D), correlated to T2i at the top of Trench 2; there is a gap between layers b and d, with the lowest sample in layer d (T2-10) weakly reversed, as might be expected for a transition to reversed from an underlying normal. Most of the samples from the lower layers a and b (all equivalent to T2hs) are normal, but the lowest three at the base of layer a are reversed. Three higher samples in a and one at the base of b are normal. Above these is a single sample (T2-8) which seems definitely reversed, but perhaps it is transitional or represents a minor "flip" within the magnetozone, and above it is sample T2-9, which is clearly normal. Trench 1 is entirely reversed, spanning most of Layer T2h (T2hs-T2hm-T2hi), but with an isolated sample at its base correlated to T2g (Fig. 5.5A).

In Trench 2 itself (Fig. 5.5B), the highest level sampled for magnetic signal is T2hs, and its upper part is normal. The lower part of T2hs, T2hm and T2hi down to sublayer 9 is all reversed. The SEN 1 tephra dated to 2.12 ± 0.03 Ma derives from the upper part of T2hi. The section in Zone H8 (Fig. 5.5C), correlated to T2hi 4–5 and 9–13, overlaps the lower part of Trench 2 and is similarly reversed. The small segment of Trench 2 in place (T2a-e) enclosing the SEN 8 tephra dated to 2.18 ± 0.05 Ma is also reversed. This results in a simple pattern of reversed above short normal (in layer T2hs) above reversed.

There are two questions about this inferred pattern: In the pit at the north of P233, sample T2-8 seems to be strongly reversed within the normal magnetozone; could this reflect transitional behavior of the field or a minor reversal? Trench 1 spans most or all of the T2hs equivalent where the normal magnetozone occurs in Trench 2 and the pit, but it is all clearly reversed. If the normal magnetozone is a short-lived interval (as we suggest below), perhaps it was not recorded in the sediments of Trench 1 as a result of stochastic processes.

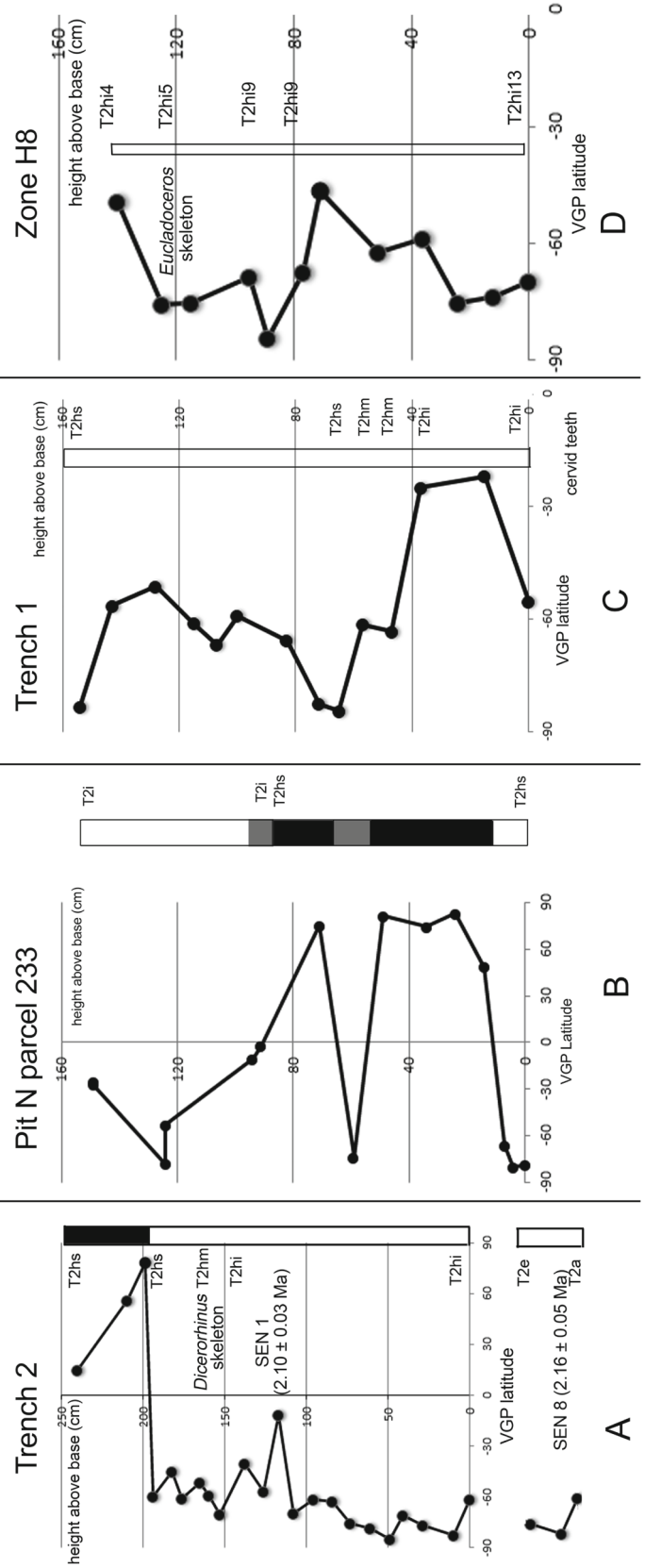

Fig. 5.5 Paleomagnetic "columns" of the western sector with vertical scale, calculated VGP latitudes and correlations of layers to those of Trench 2. A, Trench 2 (2001), normal at top and reversed below, with *Dicerorhinus* skeleton in T2hm and dated tephra SEN 1 high in T2hi; a short reversed paleomagnetic section was sampled in a small block from the base of the trench, enclosing dated tephra SEN 8. B, pit at the north end of parcel 233 (2004), with upper and lower reversed magnetozones bounding normal zone, with strong and weak reversed samples suggesting possible transitional behavior gray). C, Trench 1 (2001), entirely reversed, with cervid teeth recovered below lowest paleomagnetism sample. D, Zone H8 (2004), entirely reversed through most of T2hi equivalent, with cervid skeleton in the upper part

In parcel 172, two segments of Trench 5 yielded signal (Fig. 5.6). The highest two samples in T5 inf were reversed; eleven of the next 13 samples were probably normal, with two apparently reversed samples (T5-21 and especially T5-22) in the middle. The remaining samples in T5 inf and all those in T5 sup (stratigraphically lower) were reversed. A possible interpretation is that the field was reversing during the time represented here, with an early transitional zone, followed by a short fully(?) reversed interval and then a later transitional zone before the field stabilized as normal. The pattern appears broadly similar to that from the western sector, with a short normal and transitional zones between two reversed segments. The dated tephra SEN 101 and SEN 98, however, indicate that the majority of this section is older than what is known from the western sector.

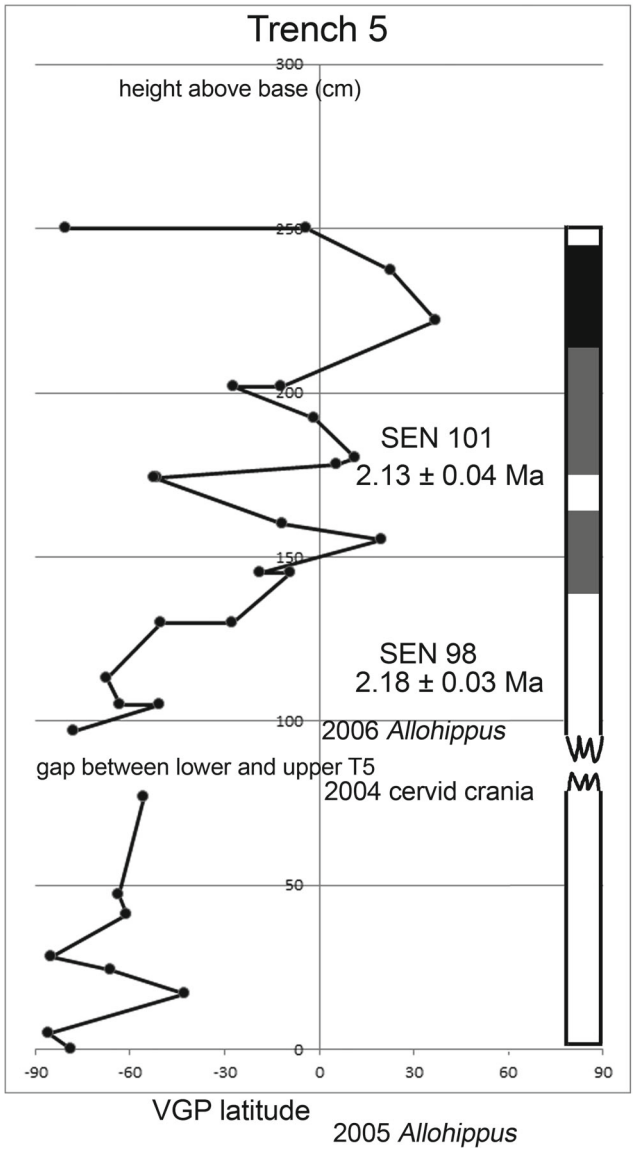

Fig. 5.6 Paleomagnetic "column" of Trench 5 in the southeastern sector (2004) with vertical scale, calculated VGP latitudes and approximate positions of dated tephra and major fossils. The normal magnetozone near the top is preceded by an apparently transitional zone (in gray); the long reversed zone below may be "interrupted" by another transitional zone. Note that the lower segment (inf) of T5 is stratigraphically above the upper segment (sup) due to local dip. The two segments have been plotted together with a gap of 20 cm placed between them; this gap is indicated on the paleomagnetic column by ragged edges

Combined ESR and U-series Analyses on Teeth

A combined Electron Spin Resonance (ESR) and Uranium-series (U-series) approach was also attempted on several teeth from parcels 172 and 233. Unfortunately, the obtained ESR/U-series ages are severely underestimated by comparison with both paleontological and $^{40}Ar/^{39}Ar$ data, supported by paleomagnetic correlation (see details of the ESR/U-series protocol and results in the Appendix). At Senèze, both relatively early U-uptake history reconstructed from the analytical data and high dose rates linked to the volcano-sedimentary context seem to prohibit the use of the ESR/U-series method.

Integrated Geochronology

Channell et al. (2020) have provided the most up to date review of geomagnetic reversals and excursions in the Early Pleistocene. In brief, for the time frame between 2.20 and 2.00 Ma, where the Senèze ages fall, they interpret data from sedimentary records and argon ages on volcanics to suggest three intervals of normal polarity, with some uncertainty due to complex correlation across great distances. The oldest of these is documented in lava flows on Réunion Island dated by $^{40}Ar/^{39}Ar$ to 2.19 ± 0.01 Ma (recalculated). This was previously known as the Réunion II (or "older Réunion") subchron, but Channell et al. (2020: 20) term it the Réunion excursion. Slightly younger in the record is a longer normal interval which was previously termed the Réunion I ("later" or "younger" Réunion) subchron, but is now renamed the Feni subchron (Singer 2014: 29; Channell et al. 2020: 20; Chron C2A.n1). Its age is slightly unclear, depending on the deep-sea drill site from which the dates are derived: either 2.14–2.09 or 2.137–2.116 ± 0.005 Ma. Ogg (2020) suggested 2.140–2.116 ± 0.005 Ma, which is accepted here. Finally, an even younger normal excursion, the Huckleberry Ridge, dates to 2.071 ± 0.003 Ma (recalculated); or 2.07 ± 0.01 Ma if typical argon uncertainties are included. With this terminology, Roger et al.'s (2000) date, recalculated to 2.12 ± 0.01 Ma, would have been within the Feni (and near its end, as they thought).

Using the argon dates from Senèze as a framework, the above results indicate that the youngest horizon, well above any fossiliferous level, dates to about 2.07 Ma (sample SEN 56). Unfortunately no paleomagnetic samples were taken nearby, but the level involved is correlated to layer T2i in trench 2, in turn correlated to layer e high in the pit at the northern edge of parcel 233, which has yielded a reversed signal. In that pit and at the top of trench 2 some 30–50 cm above the *Dicerorhinus* skeleton, there is a normal signal which probably equates to the Huckleberry Ridge excursion. It is above SEN 1, which is located about 30–50 cm below the rhino and dated at 2.10 ± 0.03 Ma in a reversed interval. Given this error range, SEN 1 must actually lie between 2.07 and 2.13 Ma, which is too young to fall below the Feni normal Subchron, but it must fit above the Feni and below the Huckleberry Ridge excursion; its real age would lie between 2.116 and 2.070 Ma. Therefore, the normal magnetozone must correlate to the Huckleberry Ridge (Fig. 5.7), despite its approximately 40 cm thickness in Trench 2 (Table 5.4). The complex alternation of normal, reversed and possible transitional geomagnetic intervals in the pit north of 233 makes it difficult to correlate zones precisely but suggests that the main normal segments equate to the Huckleberry Ridge as well.

Lower in the pit and in trenches 1 and 2, the remaining sediments are reversed. Fossils including a *Eucladoceros* skeleton, *Metacervoceros* teeth and other cervid remains were recovered below that dated tephra. The small segment of in situ sediment at the base of trench 2 is also reversed and dated 2.16 ± 0.05 Ma (SEN 8), thus presumably older than the Feni (Fig. 5.7). On the other hand, it is just possible (within error) that this block is younger than the Feni. The parcel 233–234 sequence as a whole (above T2a-T2e) therefore probably dates between about 2.15 and 2.07 Ma, with known fossils postdating the Feni subchron and predating the Huckleberry Ridge excursion; they would thus date between 2.11 and 2.07 Ma, or probably ca. 2.10–2.08 Ma if we allow some time on either side of this interval for the "empty" part of the column.

In parcel 172, as discussed above, the section is reversed at the top (in the upper part of T5 inf, see Fig. 5.8). Lower in T5 inf, there is a normal magnetozone above tephra sample SEN 101, dated 2.13 ± 0.04 Ma. This normal interval would equate to part of the Feni subchron. Below the fully

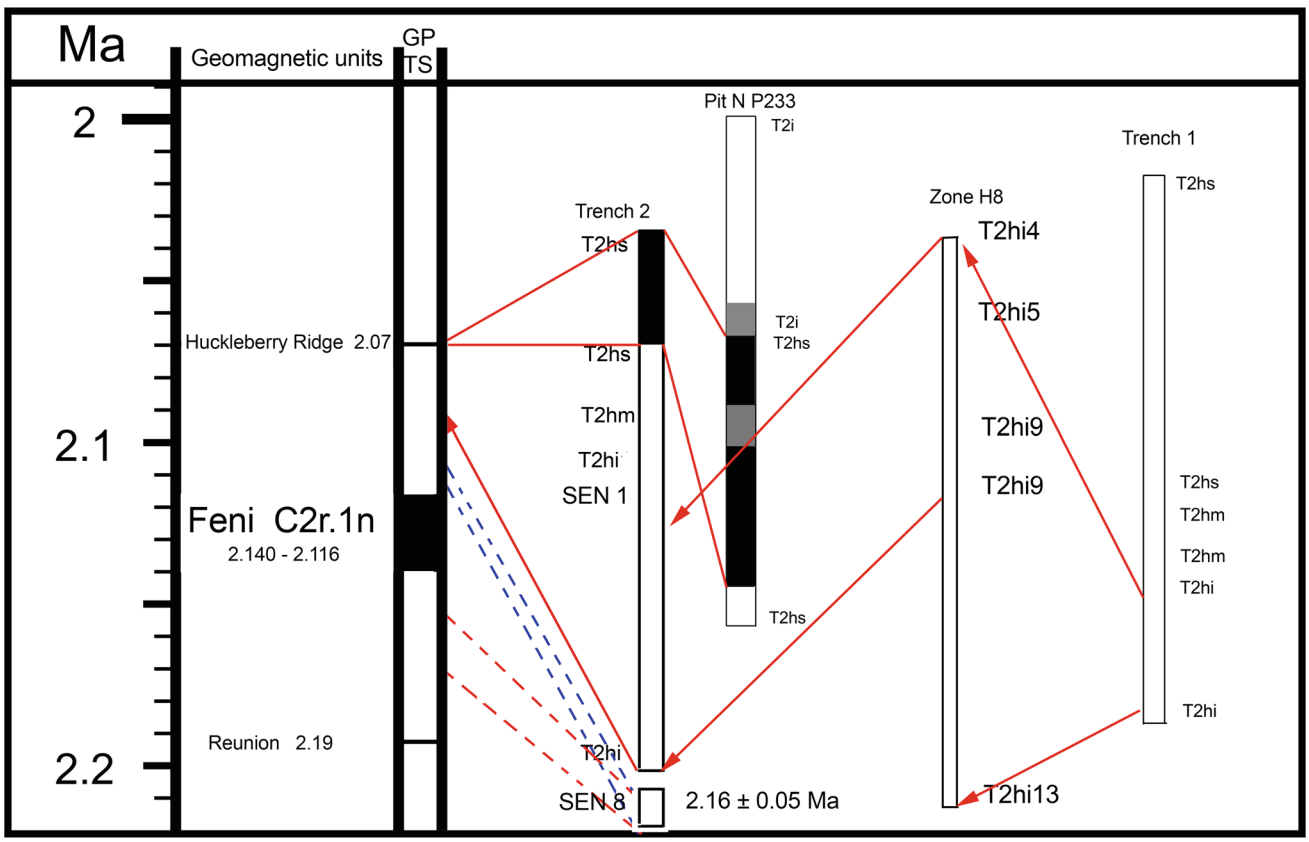

Fig. 5.7 Summary of western sector geochronology, on the Geomagnetic Polarity Time Scale (GPTS) from 2.2 to 2.0 Ma. Paleomagnetic polarity columns from Fig. 5.5, with suggested correlations to the GPTS (and each other). Solid red lines indicate approximate correlations; arrowheads indicate very broad correlation in that area. For lower block of Trench 2, dashed red lines indicate preferred possible correlations, while dashed blue lines represent a less likely option

normal interval, we have suggested that there is a zone of transition from reversed to normal with several questionable (and one clear) reversed samples in the middle (see Fig. 5.6 and Table 5.4). The upper transitional interval, which includes SEN 101, could represent the earlier part of the Feni, which begins ca. 2.14 Ma, continuing into the normal interval. It is possible that this transitional plus normal zone might instead equate to the Huckleberry Ridge excursion if the actual age of SEN 101 were between 2.11 and 2.09 Ma (at the limit of the error range). This seems unlikely, especially given that the upper transitional plus normal magnetozone(s) spans about 0.67 m of sediment, nearly twice the thickness of the Trench 2 normal (see Table 5.4 and Figs. 5.5 and 5.6). Farther down section is the lower transitional interval and then a long reversed magnetozone interpreted to be (part of) the reversed interval (C2r.2r) between the Feni and the (unobserved) Réunion excursion (2.19 Ma).

Near the top of this reversed magnetozone is the SEN 98 tephra, dated 2.18 ± 0.03 Ma. The true age of SEN 98 must lie between 2.21 and 2.15 Ma, thus older than the Feni no matter to which global polarity zone the overlying normal is equated. Even lower in the reversed zone are the two partial *Allohippus* skeketons (and also a partial cervid cranium and other specimens), whose exact ages are unknown but

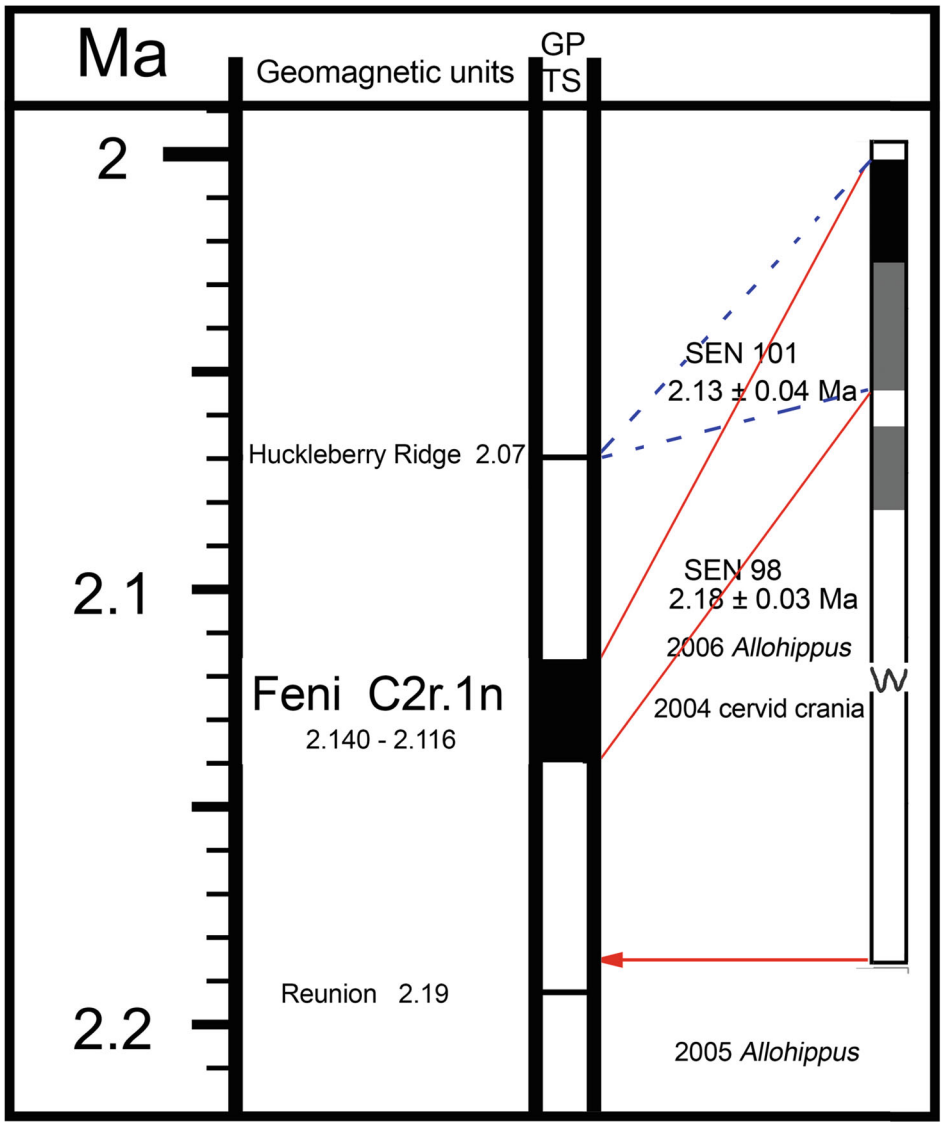

Fig. 5.8 Summary of southeastern sector (parcel 172, Trench 5) geochronology, on the Geomagnetic Polarity Time Scale (GPTS) from 2.2 to 2.0 Ma. Paleomagnetic polarity column, argon-argon ages and major fossil finds from Fig. 5.6, with suggested correlation to GPTS in red; arrowhead indicates a very broad correlation in that area; dashed blue lines indicate possible but unlikely alternative correlation. The upper middle part of the sequence is interpreted as a transition from reversed to normal, with the lower transitional zone part of the reversed interval, the upper transitional zone representing the earlier part of the Feni subchron and the fully normal zone later in the Feni. The gap between the lower (inf) portion of Trench 5 above and the upper (sup) portion below is indicated by the wavy line

probably lie between 2.20 and 2.18 Ma. The earlier suggestion (Delson et al. 2006; Nomade et al. 2014) that the younger of the skeletons was bracketed by the SEN 101 and SEN 98 ages was a misinterpretation of the preliminary analysis. This fossiliferous interval must be somewhat older than the oldest stratigraphic level in parcel 233. The parcel 172 section thus spans from about 2.20–2.11 Ma (possibly 2.08 Ma), with fossils at least between ca. 2.20 and 2.18 Ma, but probably not above this.

Combining data from the two sectors, sediments from the Senèze maar span ca. 2.20–2.07 Ma. Broadly speaking, the Senèze local fauna derives from the time interval between 2.20 and 2.10 Ma.

In our fieldwork, there seem to be two main fossiliferous horizons ca. 2.20–2.18 and 2.10–2.08 Ma (Fig. 5.9). These may represent actual intervals of faunal presence or they may reflect local lenses or clusters of fossils which we recovered, with no fossils located between them. But we don't know if the material recovered by Philis corresponds to these intervals, to the entire time span from 2.20 to 2.08 Ma or an even longer span not sampled by our work. No faunal change can be observed between these two levels, nor is any expected, mainly because there are few fossils involved and few taxa found in both "horizons", but also because the time separating them is only 100 ka. Crégut-Bonnoure (2024) does note some variation in several bovid species within the

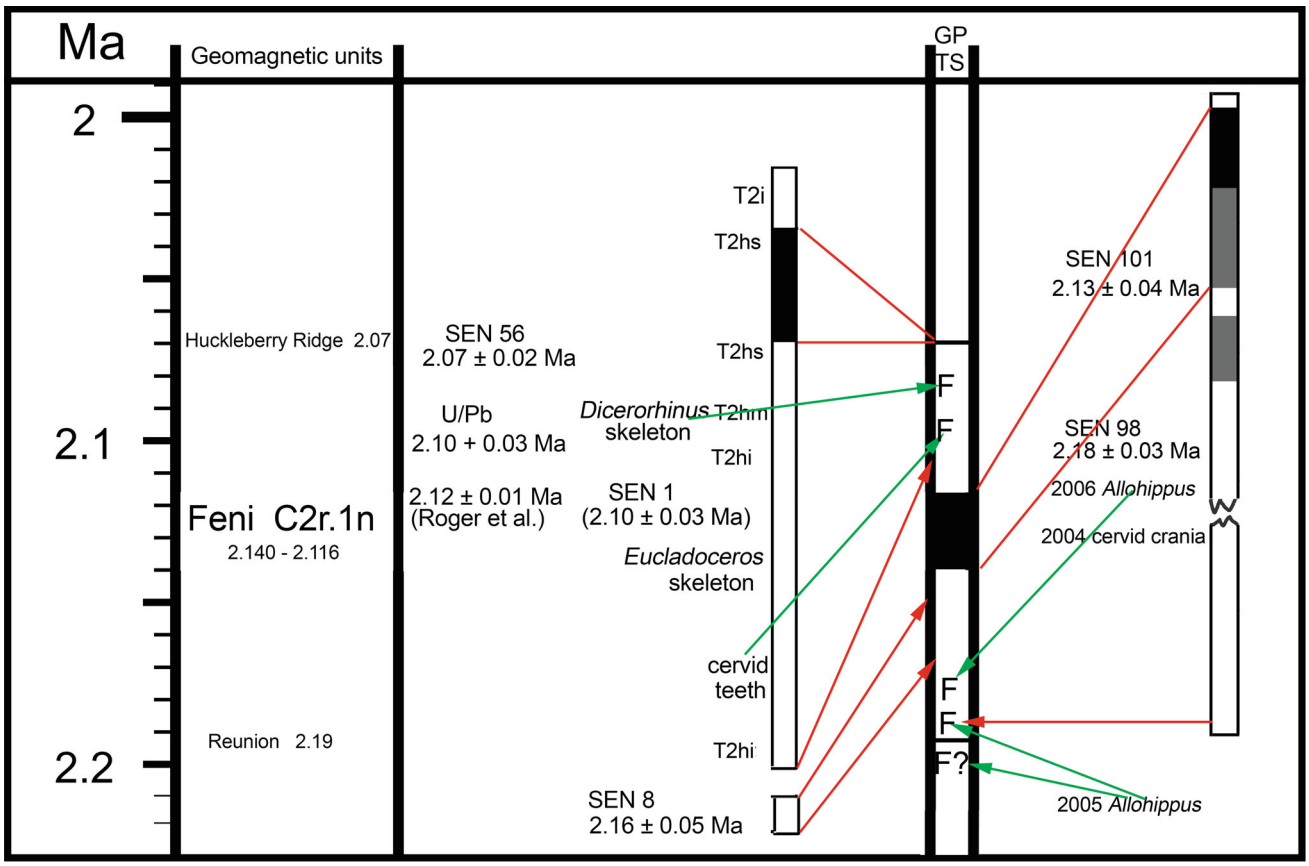

Fig. 5.9 Overview of Senèze geochronology, on the Geomagnetic Polarity Time Scale (GPTS) from 2.2 to 2.0 Ma; names of normal intervals in the GPTS column indicated at far left. The right column repeats the southeastern sequence of Trench 5 from Fig. 5.8, with suggested correlations to the GPTS in red; the arrowhead indicates a very broad correlation in that area; alternative correlation of the normal/transitional interval to the Huckleberry Ridge excursion indicated in Fig. 5.8 is not repeated here, as it is thought far less likely. The gap between the lower (inf) portion of Trench 5 above and the upper (sup) portion below is indicated by the wavy line. The green lines (with arrowheads indicating uncertainty) show possible correlation of individual fossil finds to the GPTS. The "F`s in the GTPS column indicate the fossiliferous interval, the lowest showing the possible position of the 2005 *Allohippus* skeleton below the Réunion excursion. Names of dated tephra indicate approximate position in Trench 5 section. The middle column is a composite of the four western sector sequences in Fig. 5.7 with suggested correlations to the GPTS in red (arrowheads indicate broad correlations). The green lines and F's in the GPTS column as for the southeastern sector above. Names of dated tephra indicate approximate position in Trench 2 section. At far left are three additional dates (broadly within the western sector) in their approximate chronological positions. SEN 56 is a tephra from section A, correlated to layer T2i at the top of Trench 2 (and the pit at the northern edge of parcel 233); most of section A has slid down from the top of the local sequence to a lower altitude, but the date confirms its young age. The U/Pb date was published by Paquette et al. (2021) for a horizon said to be near the top of the local sequence, but it fact it derives from section A, although from an unknown level. The argon-argon age of 2.12 Ma (recalculated here) was obtained by Roger et al. (2000) on a tephra layer within a normal magnetozone in the 1989 core. It would appear to correlate with part of the Feni subchron. All of these dates agree well with their stratigraphic positions.

Senèze sample collected by Philis, but the cause is not clear. Moreover, one specimen of *Bison* (*Eobison*) sp. (Crégut-Bonnoure 2024) and one of *Allohippus major* (Eisenmann & Delson 2024) were recovered from parcel 164 (as surface finds) and donated to the team by local collector A. Consigny; the *Bison* probably indicates the presence of a significantly younger fossil horizon (Epivillafranchian?) not otherwise sampled.

Three other ages may be added to the picture (Fig. 5.9). Tephra SEN 56, from section A in parcel 234, derives from high in the Senèze sequence (Debard 2024), as confirmed by the date of 2.07 ± 0.02 Ma. From an uncertain level in section A, Paquette et al. (2021) obtained a U/Pb date (rounded to two decimal places) of 2.10 ± 0.03 Ma. These are equivalent within error. Finally, Roger et al. (2000) dated a tephra within a normal magnetozone in the 1989 core, and we have recalculated that age to 2.12 ± 0.01 Ma, within the Feni and presumably equivalent to the normal zone in the Trench 5 sequence. Most of the pollen samples from the 1965 core must predate most or all of the Senèze fauna collected by our team (see also Argant 2024).

Summary and Conclusions

The Senèze maar (Haute-Loire, central France) has yielded fossil mammals since 1892. It has long been considered to date to the Late Pliocene, modified to Early Pleistocene following the redefinition of the Plio-Pleistocene boundary to 2.58 Ma. The first chronometric date for Senèze was provided by Prévot and Dalrymple (1970), who published a K–Ar age of 2.30 Ma for the underlying basalt marking the opening of the maar. The normal magnetozone they discerned in the 1965 core was equated to the Réunion "1" (now Feni) subchron. The $^{40}Ar/^{39}Ar$ ages on tephra from the Senèze sequence published by Nomade et al. (2014) were recalculated to conform to current standards. Samples for paleomagnetic analysis were collected by S.S. in 2001 and 2004 and are analyzed here.

The investigation by Bahain et al. (Appendix) has revealed that dating by ESR and U-series methods is especially problematic in the earlier Early Pleistocene. Only in cases where favorable conditions of late uptake and low environmental radioactive dose rate prevail would such dating succeed. Both these conditions are unfavorable at Senèze, resulting in ESR dates younger than or close to 1 Ma, far younger than those obtained via $^{40}Ar/^{39}Ar$ dating and confirmed with paleomagnetic correlation.

The Senèze deposits probably span most of the time between the Huckleberry Ridge and Réunion excursions, ca. 2.20–2.07 Ma (see Fig. 5.9). The western sector in parcels 233 and 234 (especially Trench 2) spans roughly 2.15–2.07 Ma. A normal magnetozone high in the sequence is correlated to the Huckleberry Ridge excursion at 2.07 Ma. The Feni subchron was apparently not sampled, but a date of 2.16 ± 0.05 Ma on a lower segment of Trench 2 suggests that it occurred within the time interval represented in the sector. Major fossil finds include a partial skeleton of *Dicerorhinus etruscus etruscus*, a partial skeleton of *Eucladoceros ctenoides senezensis* and teeth of *Metacervoceros rhenanus philisi*, which derive from a fossiliferous level dated ca. 2.10–2.08 Ma.

The southeastern sector in parcel 172 (especially Trench 5) appears to span from ca. 2.20–2.11 (or 2.08) Ma. A short reversed interval at the top of the paleomagnetic "column" postdates the Feni subchron (2.140–2.116 Ma). A normal magnetozone is preceded by a transitional complex which may include part of the Feni at the top and then the pre-Feni reversed interval (C2r.2r). There is no indication of the Réunion excursion, which may predate the entire sequence or might possibly be located below the lowest paleomagnetic sample. The stratigraphically constrained faunal remains in this sector (including two partial skeletons of *Allohippus senezensis* from Trenches 6 and 7) range from just below the SEN 98 tephra dated 2.18 ± 0.03 Ma through the lower reversed magnetozone and below it, thus ca. 2.20–2.18 Ma, but no younger than 2.15 Ma (the youngest age of SEN 98 within error). Those two equid skeletons were not located between dated samples SEN 98 and SEN 101, as incorrectly suggested by Delson et al. (2006) and Nomade et al. (2014). Instead both are older than these dated tephra, and the older of them lies below the oldest paleomagnetic sample. The position of that skeleton with regard to the Réunion excursion is unknown: it could lie above, within or below that (unsampled) short normal interval.

Senèze is a pivotal site in the sequence of western European mammalian faunal evolution. It has been recognized as the reference locality for both the Late Villafranchian land mammal age and the MNQ 18 regional mammal unit (see Crégut-Bonnoure et al. 2024). The age of this site is now known accurately, because Senèze is one of the few European later Cenozoic localities with a tightly developed stratigraphic context which has yielded both $^{40}Ar/^{39}Ar$ ages and paleomagnetic data which help to tie down the dating. Study of additional such well-documented fossil sites will further establish precise dating of the European Plio-Pleistocene mammalian biochronology.

Acknowledgments We thank Martine Faure and Claude Guérin for field support during sampling and for organization of the entire Senèze project. We thank Messieurs Didier Miallier et Jean Fain, of the Laboratoire de Physique Corpusculaire de l'Université Blaise Pascal—Clermont Ferrand II, for the loan of a gamma spectrometer; and Madame Hélène Valladas, then of the Centre des Faibles Radioactivités, Laboratoire mixte CNRS-CEA, Gif sur Yvette, for the loan of several TL dosimeters; these devices were used by Bonnie Blackwell in

her attempt to obtain an ESR age for Senèze. Advice on the interpretation of paleomagnetic data was given to Delson by the late Frank Brown, John Kappelman and Chris Lepre. We used the TimeScale Creator program (https://timescalecreator.org/index/index.php) to make several of the figures. We thank Eric Sargis, an anonymous reviewer and especially Isaac Casanovas-Vilar for comments on earlier drafts of this manuscript.

Appendix: Attempted Combined ESR and U-series Dating of Tooth Enamel from Senèze

Jean-Jacques Bahain, Qingfeng Shao and Christophe Falguères.

A combined Electron Spin Resonance (ESR) and Uranium-series (U-series) approach was applied at the Muséum national d'Histoire naturelle (MNHN), Paris, on several teeth excavated from the different areas of Senèze to investigate the success of this approach on fossils of a known Early Pleistocene age. The combination of these two methods allows a better evaluation of post-mortem uranium-uptake into the dental tissues and associated variations of the dose rate over time. This phenomenon, which depends on the nature of the site and the age of the sample, makes the determination of the ESR ages (strongly linked to uranium content) particularly delicate, and it is necessary to use mathematical models to describe the evolution of this parameter over time. In order to calculate the age of a given sample, the various data acquired through ESR and U-series analyses are used together to model the post-mortem U-uptake in the different tissues (US model with "p" U-uptake parameter, Grün et al. 1988) and in some cases a late loss of uranium (leaching, AU model with "n" U-uptake parameter, Shao et al. 2012; see Fig. 5.A1). One of the main interests of this approach is to allow the determination for each dental tissue of a U-uptake parameter calculated from the whole set of analytical data and hence the description of the uranium-uptake kinetics into the considered tissue.

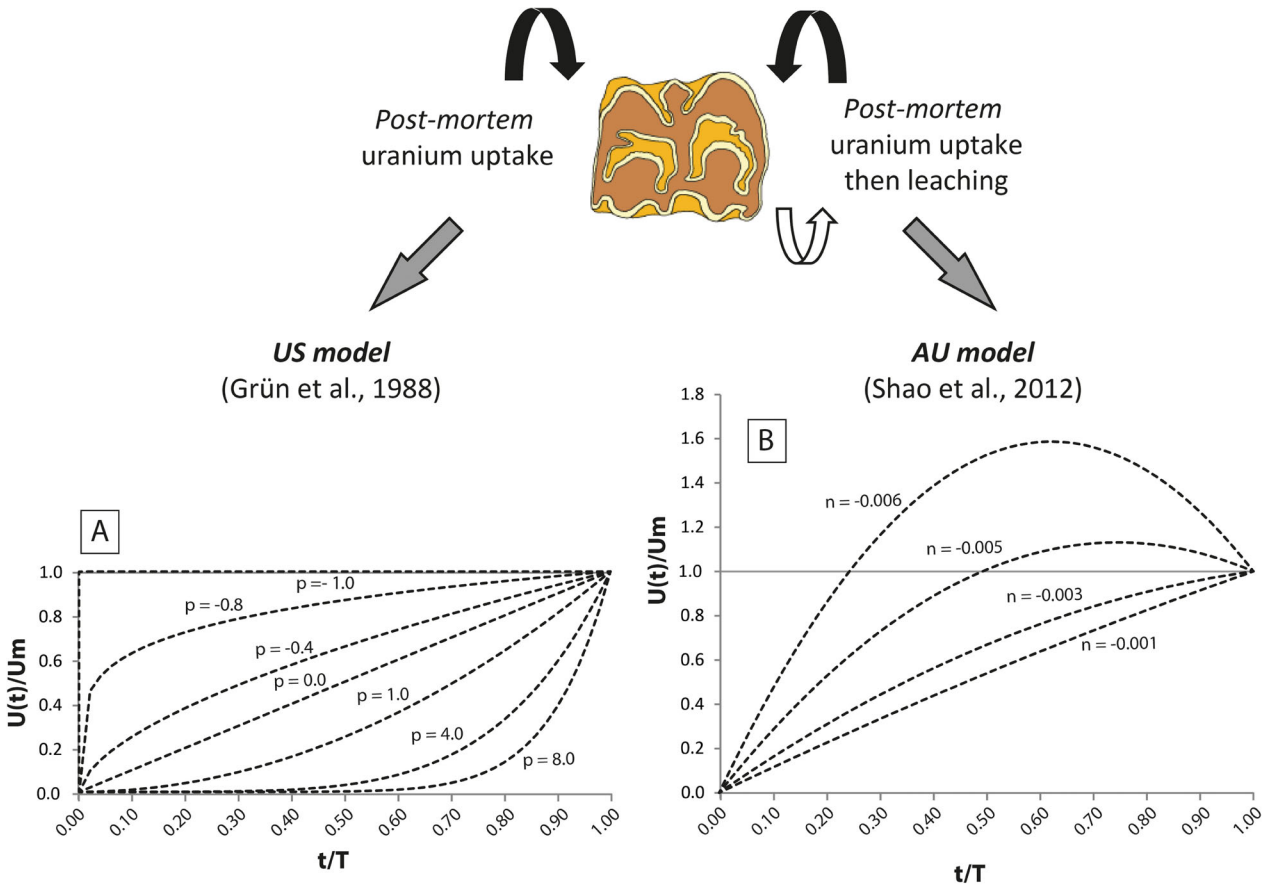

Fig. 5.A1 Kinetics of the uranium uptake in a given paleontological tissue as a function of the determined U-uptake parameter (A: incorporation only, p-parameter, US model, Grün et al. 1988; B: incorporation then leaching, n-parameter, AU model, Shao et al. 2012). U(t) is the uranium content in a tissue at time t, Um is the current uranium content in this tissue, T is the age of the sample

MNHN Laboratory Analytical Method

The Senèze teeth were prepared following the protocol described by Bahain et al. (2020). After mechanical separation of the dental tissues, the enamel was cleaned using a dental drill to remove any contamination of sediment or dentine. For the calculation of the beta contribution, the enamel thickness was measured before and after enamel preparation on both sides. The enamel was then ground and sieved. ESR study was then conducted by the additive method. The 100–200 µm enamel fraction was split in ten aliquots, nine of them were irradiated by a γ ^{60}Co source at doses ranging from 260 to 11,700 Gy. The ESR intensity of each aliquot was then measured using a Bruker© EMX ESR spectrometer, and a dose–response curve was built from the data set for the tooth. Palaeodoses, D_e, were determined using an exponential + linear function (E + L) (Shao et al. 2015). Radioelement contents of the dental tissues and associated sediments were measured by γ-ray spectrometry, and U-series analyses were performed on each dental tissue. The γ dose was recorded on the field by TL dosimeters *in situ* at different points in Trench 2 around the level of the rhino skeleton. Additional laboratory gamma measurements were performed on several sediment samples from the same level.

U-series analyses were then realized at Nanjing Normal University, China, on a Neptune Multi-Collector Inductively Coupled Plasma Mass Spectrometer (MC-ICPMS) (see details of the chemical and analytical protocols in Shao et al. 2019). Lastly, dose rates (D_a) contributions, U-uptake parameters and ESR/U-series ages were calculated from both ESR and U-series data applying either the US model (Grün et al. 1988) or the AU model (Shao et al. 2014), according to their isotopic characteristics.

Results of ESR/U-Series Analyses

The results are presented in Appendix Table 5.A1 (U-series data) and Appendix Table 5.A2 (ESR/U-series data). The U content in enamel and dentine ranges from 0.8 to 5.0 ppm and 52.5 to 82.1 ppm, respectively. These relatively high U-content values are associated with systematically high ^{230}Th/^{234}U ratios, mainly higher than 1.00, often too high to permit the use of the US model. On the other hand, the equivalent doses (D_e) are surprisingly relatively low, between 2000 and 3100 Gy, and the combination of these parameters leads to dental tissue dose being the most important factor in the age calculation.

The ESR/U-series ages, ranging from 686 ± 59 ka to 965 ± 75 ka, were obtained using the AU model for three teeth. Unfortunately, the whole set of ages is severely underestimated by comparison with both paleontological and ^{40}Ar/^{39}Ar data. Even if the values are relatively low, the higher the enamel U-content, the lower the age estimate.

As the same environmental dose was used for all the teeth and in order to evaluate if the age underestimation could be related to a poor dosimetric reconstruction, an isochron plot was fitted to the obtained data (Fig. 5.11). Despite a relatively good fit indicating that the dose reconstruction seems correct, the isochron age estimate is older (around 1047 ka), but it is still significantly lower than the ^{40}Ar/^{39}Ar age estimate. The dosimetric reconstruction therefore seems correct but cannot explain the age underestimation. It appears instead that the observed age underestimation of the Senèze teeth could be linked to the determination of the equivalent dose rather than to the dosimetric history of the samples.

This confirms the observations of Joannès-Boyau and Grün (2011) who argued that the enamel ESR signal would be composite with at least one unstable component leading to such age underestimation. The dating of earlier Early Pleistocene deposits by this method would thus be compromised except in favorable conditions (late uptake history in the dental tissues and low environmental radioactivity context), such as at Longgupo, China (Han et al. 2017). At Senèze, both relatively early U-uptake history and high dose rates seem to prohibit the use of the ESR/U-series method.

Table 5.A1 U-series data (MC-ICP-MS) obtained on fossil teeth from Senèze

Sample	Tissue	U (ppm)	Isotopic ratios				U-series apparent ages (ka)
			$^{234}U/^{238}U$	$^{230}Th/^{232}Th$	$^{230}Th/^{234}U$	$^{222}Rn/^{230}Th$	
SEN12 (P233-2004–04-0012)	Enamel	3.583 ± 0.015	1.153 ± 0.004	>100	0.960 ± 0.005	1.00	280.2 ± 7.5
	Dentine	82.140 ± 0.291	1.268 ± 0.004	>1000	1.043 ± 0.006	1.00	382.8 ± 17.4
SEN102a (P172-2006–06-0102)	Enamel	2.321 ± 0.009	1.128 ± 0.005	>1000	0.951 ± 0.005	1.00	275.8 ± 7.5
	Dentine	52.513 ± 0.195	1.121 ± 0.003	>1000	1.001 ± 0.006	0.92	377.3 ± 18.4
SEN102b (P172-2006–06-0102)	Enamel	0.807 ± 0.001	1.233 ± 0.002	>100	1.022 ± 0.003	1.00	350.9 ± 7.0
	Dentine	57.648 ± 0.150	1.120 ± 0.002	>1000	1.036 ± 0.005	1.00	535.1 ± 57.9
SEN253 (P233-2004–04-0253)	Enamel	2.190 ± 0.005	1.177 ± 0.003	>100	0.939 ± 0.004	1.00	252.4 ± 3.8
	Dentine	68.211 ± 0.272	1.277 ± 0.005	>1000	1.091 ± 0.007	0.68	681.3 ± 12.7
SEN346 (P172-2004–04-0346)	Enamel	4.983 ± 0.011	1.205 ± 0.003	>1000	0.987 ± 0.004	1.00	301.3 ± 5.4
	Dentine	78.815 ± 0.268	1.206 ± 0.004	>1000	1.034 ± 0.006	0.87	395.9 ± 18.9

Notes SEN12 and SEN253 are cheek teeth of *Dicerorhinus etruscus*, SEN102a and SEN102b are incisors of *Allohippus senezensis* and SEN346 is a cheek tooth of *Eucladoceros ctenoides*; P172 and P233 refer to the parcels from which the teeth were recovered; the 6-digit number is the field catalog number, formally FSL SEN 04-0012, etc. Uncertainties for isotopic ratios and ages are given with ±2σ. The eventual radon (Rn) losses were determined for each tissue by combining α and γ spectrometry data (Bahain et al. 1992)

Table 5.A2 ESR/U-series data obtained on fossil teeth from Senèze

Sample	Tissue	Equivalent doses D_e (Gy)	U uptake parameters p (US) or *n* (*AU*)	Annual dose rate contributions (μGy/a)				ESR/U-series ages–US or *AU* (ka)
				α	β	γ + cosmics	Total	
SEN12 (P233-2004-04-0012)	Enamel	2843 ± 184	−0.563 ± 0.038	1319 ± 292	763 ± 147	1120 ± 55	3202 ± 332	***888 ± 72***
	Dentine		*−0.0012 ± 0.0001*					
SEN102a (P172-2006-06-0102)	Enamel	2097 ± 124	−0.529 ± 0.042	800 ± 208	477 ± 96	1120 ± 55	2397 ± 236	**875 ± 69**
	Dentine		−0.851 ± 0.003					
SEN102b (P172-2006-06-0102)	Enamel	2078 ± 79	−0.891 ± 0.003	385 ± 110	649 ± 139	1120 ± 55	2154 ± 186	**965 ± 75**
	Dentine		−0.001 ± 0.001					
SEN253 (P233-2004-04-0253)	Enamel	2334 ± 68	−0.408 ± 0.042	726 ± 125	815 ± 129	1120 ± 55	2659 ± 186	***878 ± 56***
	Dentine		*−0.0012 ± 0.0001*					
SEN346 (P172-2004-04-0346)	Enamel	3050 ± 235	−0.757 ± 0.026	2161 ± 469	1169 ± 206	1120 ± 55	4446 ± 514	***686 ± 59***
	Dentine		*−0.0016 ± 0.0001*					

Notes Sample identifications, see Table 5.A1. Ages were calculated taking into account the effects of sample preparation on the beta dose rate contributions (Brennan et al. 1997). Uranium uptake parameters and ESR/U-series ages are presented in italics if n (for the AU model) or not bold if p (for the US model). Dose rate contributions (alpha, beta, gamma + cosmic and total) were calculated using conversion factors from Guérin et al. (2011). The γ-dose used for the age calculation corresponds to the mean value of the doses recorded by TL dosimeters. The β-sediment dose rate was calculated from the uranium, thorium and potassium contents of the paleontological layer, and the cosmic dose rate was determined from the depth of this level using the equations given by Prescott and Hutton (1994). A k-value of 0.13 ± 0.02 was used in the α-dose rate calculation (Grün and Katzenberger-Appel 1994). The water content was estimated to be 0 wt% in the enamel, 7 wt% in the dentine and 18 wt% in the sediment. The ESR/U-series ages were calculated with the "ESRUS" and "ESRAU" Matlab routines written by Qingfeng Shao, and the ages are given with ± 1 sigma

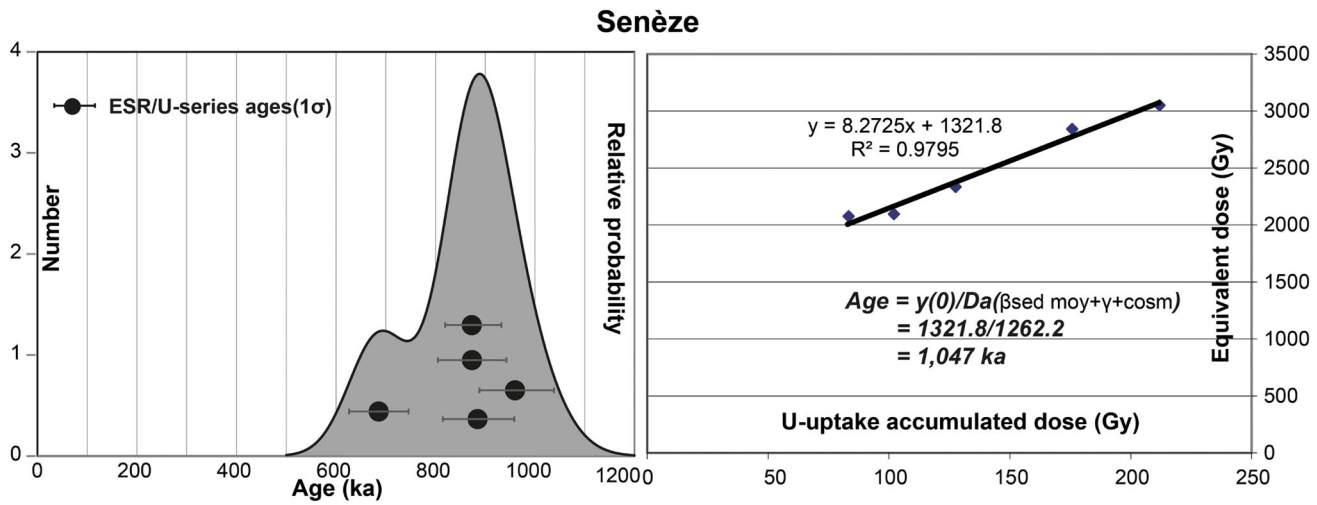

Fig. 5.A2 Probability plot (left) and isochron plot (right) of the ESR/U-series data obtained on fossil teeth from Senèze

References

Azzaroli, A. (1970) Villafranchian correlations based on large mammals. *Giornale di Geologia, 35*, 1–21.

Azzaroli, A., de Giuli, C., Ficcarelli, G., & Torre, D. (1988). Late Pliocene to early Mid-Pleistocene mammals in Eurasia: Faunal succession and dispersal events. *Palaeogeography, Palaeoclimatology, Palaeoecology, 68*, 77–100.

Bahain, J.-J., Yokoyama, Y., Falguères, C., & Sarcia, M. N. (1992). ESR dating of tooth enamel: A comparison with K-Ar dating. *Quaternary Science Reviews, 11*, 245–250.

Bahain, J.-J., Duval, M., Voinchet, P., Tissoux, H., Falguères, C., Grün, R., et al. (2020). ESR and ESR/U-series chronology of the Middle Pleistocene site of Tourville-la-Rivière (Normandy, France)—A multi-laboratory approach. *Quaternary International, 556*, 66–78

Blackwell, B. A. B., Delson, E., McNulty, K., Capellini, T. D., Blickstein, J. I. B., Skinner, A. B., et al. (2020). Dosimetry and ESR analyses at Senèze, France: dating Villafranchian monkeys and associated fauna (abstract). *American Journal of Physical Anthropology, 171*(S69), 29.

Bouchez, R., Lopez Carranza, E., Ma, J. L., Amosse, J., Piboule, M., Cornu, A., et al. (1984). Datation par spectrometrie RPE d'émail dentaire fossile dans le domaine de 50,000 ans à plusieurs millions d'années. *Revue d'Archéométrie, 8*, 70–79.

Boule, M. (1892). Découverte d'un squelette d' *Elephas meridionalis* dans les cendres basaltiques du volcan de Senèze (Haute-Loire). *Comptes Rendus hebdomadaires des Séances de l'Academie des Sciences*, *115*, 624–626.

Brennan, B. J., Rink, W. J., Mcguirl, E. L., Schwarcz, H. P., & Prestwich, W. V. (1997). Beta doses in tooth enamel by "One Group" theory and the Rosy ESR dating software. *Radiation Measurements, 27*, 307–314.

Channell, H. E. T., Singer, B. S., & Jicha, B. R. (2020). Timing of Quaternary geomagnetic reversals and excursions in volcanic and sedimentary archives. *Quatermary Science Reviews, 228*, 106–114.

Couthures, J. (1989) The Senèze maar (French Massif Central): Hypothesis regarding a catastrophe occurring about 1.5 million years ago. *Journal of Volcanology and Geothermal Research, 39*, 207–210.

Couthures, J., & Pastre, J.F. (1983). Chronostratigraphie du Plio-Pléistocène d'Auvergne et du Velay: Nouveaux apports des datations radiométriques et du paléomagnétisme. *Bulletin de l'Association française pour l'étude du Quaternaire*, *1983-1*, 9–18.

Crégut-Bonnoure, E. (2024). The Bovidae (Mammalia, Cetartiodactyla) from Senèze. In E. Delson, M. Faure, & C. Guérin (Eds.), *Senèze: Life in Central France two million years ago. Paleontology, geochronology, stratigraphy and taphonomy* (pp. 433–585). Cham (Switzerland): Springer.

Crégut-Bonnoure, E., Guérin, C., Argant, A., Argant, J., Debard, E., Delson, E. et al. (2024). Biochronology of the Senèze faunal assemblage. In E. Delson, M. Faure & C. Guérin (Eds.), *Senèze: Life in Central France two million years ago. Paleontology, geochronology, stratigraphy and taphonomy* (pp. 633–652). Cham (Switzerland): Springer.

Debard, E. (2024). Geological study of the Early Pleistocene site of Senèze (Domeyrat, Haute-Loire, France). In E. Delson, M. Faure & C. Guérin (Eds.), *Senèze: Life in Central France two million years ago. Paleontology, geochronology, stratigraphy and taphonomy* (pp. 37–82). Cham (Switzerland): Springer.

Delson, E., & Plopsor, D. (1975). *Paradolichopithecus*, a large terrestrial monkey (Cercopithecidae, Primates) from the Plio-Pleistocene of southern Europe and its importance for mammalian biochronology. In *Proceedings of the VIth session, Regional Committee on Mediterranean Neogene Stratigraphy*, Bratislava, 1975 (pp. 91–96). Bratislava: Slovak Academy of Sciences.

Delson, E., Faure, M., Guérin, C., Aprile, A., Argant, J., Blackwell, B., et al. (2006). Franco-American renewed research at the Late Villafranchian locality of Senèze (Haute-Loire, France). *Courier Forschunginstitut Senckenberg, 256*, 275–290.

Depéret, C. (1929). *Dolichopithecus arvernensis* Dépéret: Nouveau singe du pliocène supérieur de Senèze (Haute-Loire). *Travaux du Laboratoire de Géologie de la Faculté des Sciences de Lyon 15*, 5–12.

Depéret, C., & Mayet, L. (1912). Le gisement de mammifères pliocènes de Senèze (Haute-Loire). *Association française pour l'avancement des Sciences–Compte rendu de la 40me session–Dijon–1911–Notes et Mémoires. Mémoire hors volume*, 138–151.

Ehrlich, A. (1968). Les diatomées fossiles des sédiments villafranchiens de Senèze (Haute-Loire, Massif Central français). *Bulletin de l'Association française pour l'Étude du Quaternaire 4*, 267–280.

Eisenmann, V., & Delson, E. (2024) The Senèze equids. In E. Delson, M. Faure, & C. Guérin (Eds.), *Senèze: Life in Central France two million years ago. Paleontology, geochronology, stratigraphy and taphonomy* (pp. 307–385). Cham (Switzerland): Springer.

Faure, M., Delson, E., & Guérin, C. (2024). Introduction and history of research in the Senèze maar. In E. Delson, M. Faure & C. Guérin (Eds.), *Senèze: Life in Central France two million years ago. Paleontology, geochronology, stratigraphy and taphonomy* (pp. 1–25). Cham (Switzerland): Springer.

Grün, R., & Katzenberger-Apel, O. (1994). An alpha irradiator for ESR dating. *Ancient TL, 12*, 35–38.

Grün, R., Schwarcz, H. P., & Chadam, J. M. (1988). ESR dating of tooth enamel: Coupled correction for U-uptake and U-series disequilibrium. *Nuclear Tracks and Radiation Measurements 14*, 237–241.

Guérin, C. (2024). *Dicerorhinus etruscus etruscus* from the Late Villafranchian site of Senèze (Domeyrat, Haute-Loire, Central France). In E. Delson, M. Faure & C. Guérin (Eds.), *Senèze: Life in Central France two million years ago. Paleontology, geochronology, stratigraphy and taphonomy* (pp. 245–306). Cham (Switzerland): Springer.

Guérin, C., Faure, M., Argant, A., Argant, J., Crégut-Bonnoure, E., Debard, E., et al. (2004). Le gisement pliocène supérieur de Saint-Vallier (Drôme, France): synthèse biostratigraphique et paléoécologique. In M. Faure & C. Guérin (Eds.), *Le gisement-pliocène terminal de Saint-Vallier (Drôme, France), Geobios*, Mémoire spécial 26, 37, 349–360.

Guérin, G., Mercier, N., Adamiec, G. (2011). Dose-rate conversion factors: Update. *Ancient TL, 29*, 5–8.

Han, F., Bahain, J.-J., Deng, C., Boëda, É., Hou Y., et al. (2017). The earliest evidence of hominid settlement in China—Combined electron spin resonance and uranium series (ESR/U-series) dating of mammalian fossil teeth from Longgupo cave. *Quaternary International, 434*, part A, 75–83.

Heintz, E. (1970). Les cervidés Villafranchiens de France et d'Espagne. *Mémoires du Muséum National d'Histoire Naturelle*, Paris, *série C*, 22, volumes 1 and 2, 1–317, 1–206.

Jicha, B., Singer, B., & Sobol, P. (2016). Re-evaluation of the ages of $^{40}Ar/^{39}Ar$ sanidine standards and supereruptions in the western U.S. using a Noblesse multi-collector mass spectrometer. *Chemical Geology, 431*, 54–66

Joannes-Boyau, R., & Grün, R. (2011). A comprehensive model for CO_2-radicals in fossil tooth enamel: Implications for ESR dating. *Quaternary Geochronology, 6*, 82–97.

Mei, T. D. G, Blackwell, B. A. B., Delson, E., Frost, S., Blickstein, J. I. B., & Divjak, M. N. (2001). ESR dating the Villafranchian in France and elsewhere: A "handicapped" study? (abstract) GSA *Program with Abstracts*, 2001, poster BTH 58, A-199.

Min, K., Mundil, R., Renne, P. R., & Ludwig, K. R. (2000). A test for systematic errors in $^{40}Ar/^{39}Ar$ geochronology through comparison

with U/Pb analysis of a 1.1-Ga rhyolite. *Geochimica et Cosmochimica Acta*, *64*, 73–98.

Niespolo, E. M., Rutte, D., Deino, A. L., & Renne, P. R. (2017). Intercalibration and age of the Alder Creek sanidine $^{40}Ar/^{39}Ar$ standard. *Quaternary Geochronology, 39*, 205–213.

Nomade, S., Renne, P. R., Vogel, N., Deino, A. L., Sharp, W. D., Becker, T. A., et al. (2005). Alder Creek Sanidine (ACs-2): A Quaternary $^{40}Ar/^{39}Ar$ standard. *Chemical Geology, 218*, 319–342.

Nomade, S., Gauthier, A., Guillou, H., & Pastre, J. F. (2010). $^{40}Ar/^{39}Ar$ temporal framework for the Alleret maar lacustrine sequence (French Massif Central): Volcanological and paleoclimatic implications. *Quaternary Geochronology, 5*, 20–27.

Nomade, S., Pastre, J.-F., Guillou, H., Faure, M., Guérin, C., Delson, E., et al. (2014). $^{40}Ar/^{39}Ar$ constraints on some French landmark Late Pliocene to Early Pleistocene large mammalian paleofaunas: Paleoenvironmental and paleoecological implications. *Quaternary Geochronology, 21*, 2–15.

Ogg, J. (2020). Geomagnetic polarity time scale. In F. M. Gradstein, J. G. Ogg, M. D. Schmitz, & G. M. Ogg (Eds.), *Geologic Time Scale 2020* (pp. 159–192). Amsterdam: Elsevier.

Paquette, J.-L., Médard, E., Poidevin, J.-L., & Barbet, P. (2021). Precise dating of middle to late Villafranchian mammalian paleofaunae from the Upper Allier River valley (French Massif Central) using U–Pb geochronology on volcanic zircons. *Quaternary Geochronology*, *65*, 101198.

Parenti, F., Valli, A., Aprile, L., Candelato, F., Monguillon, A., Natali, L. et al. (2024). Surveying and excavations at Senèze: 2001–2006. In E. Delson, M. Faure & C. Guérin (Eds.), *Senèze: Life in Central France two million years ago. Paleontology, geochronology, stratigraphy and taphonomy* (pp. 27–35). Cham (Switzerland): Springer.

Pastre, J.-F. (2024). The Senèze maar and paleontological site (Massif Central, France): Their volcanic context and studies of related tephras. In E. Delson, M. Faure & C. Guérin (Eds.), *Senèze: Life in Central France two million years ago. Paleontology, geochronology, stratigraphy and taphonomy* (pp. 83–98). Cham (Switzerland): Springer.

Prescott, J. R., & Hutton, J. T. (1994). Cosmic ray contributions to dose rates for luminescence and ESR dating: Large depths and long-term time variations. *Radiation Measurements, 23*, 497–500.

Prévot, M., & Dalrymple, G. B. (1970). Un bref épisode de polarité géomagnétique normale au cours de l'époque inverse Matuyama. *Comptes Rendus de l'Académie des Sciences*, *271 D*, 2221–2224.

Renne, P. R., Swisher, C. C., Deino, A. L., Karner, D. B., Owens, T. L., & DePaolo, D. J. (1998). Intercalibration of standards, absolute ages and uncertainties in $^{40}Ar/^{39}Ar$ dating. *Chemical Geology, 145*, 117–152.

Renne, P. R., Balco, G., Ludwig, K. R., Mundil, R., & Min, K. (2011). Response to the comment by W.H. Schwarz et al. on "Joint determination of K-40 decay constants and Ar-40*/K-40 for the Fish Canyon sanidine standard, and improved accuracy for Ar-40/Ar-39 geochronology" by P.R. Renne et al. (2010). *Geochimica et Cosmochimica Acta, 75*, 5097–5100.

Roger, S., Coulon, C., Thouveny, N., Féraud, G., Van Velzen, A., Fauquette, S., et al. (2000). $^{40}Ar/^{39}Ar$ dating of a tephra layer in the Pliocene Senèze maar lacustrine sequence (French Massif Central): constraint on the age of the Réunion-Matuyama transition and implications on paleoenvironmental archives. *Earth and Planetary Science Letters, 183*, 431–440.

Schaen, A. J., Jicha, B. R., Hodges, K. V., Vermeesch, P., Stelten, M. E., Mercer, C. M., et al. (2021). Interpreting and reporting $^{40}Ar/^{39}Ar$ geochronologic data. *GSA Bulletin, 133,* 461–487.

Schaub, S. (1943). Die oberpliocaene Säugetierfauna von Senèze (Haute-Loire) und ihre verbreitungsgeschichtliche Stellung. *Eclogae Geologicae Helvetiae*, *36*, 270–289.

Shao, Q., Bahain, J.-J., Dolo, J.-M., & Falguères, C. (2014). Monte Carlo approach to calculate US-ESR ages and their uncertainties. *Quaternary Geochronology, 22*, 99–106.

Shao, Q., Bahain, J. J., Falguères, C., Dolo, J.-M., & Garcia, T. (2012). A new U-uptake model for combined ESR/U-series dating of tooth enamel. *Quaternary Geochronology,10*, 406–441.

Shao, Q., Bahain, J.-J., Wang, W., Jin, C., Wang, Y., Voinchet, P., et al. (2015). Combined ESR and U-series dating of early Pleistocene *Gigantopithecus* faunas at Mohui and Sanhe Caves, Guangxi, southern China. *Quaternary Geochronology, 30*, 524–528.

Shao, Q., Li, C., Huang, M., Liao, Z., Arps, J., Huang, C., et al. (2019). Interactive programs of MC-ICPMS data processing for 230Th/U Geochronology. *Quaternary Geochronology, 51*, 43–52.

Singer, B. S. (2014). A Quaternary geomagnetic instability time scale. *Quaternary Geochronology, 21*, 29–52.

Stehlin, H. G. (1923). Die oberpliocaene Fauna von Senèze (Haute-Loire). *Eclogae Geologicae Helvetiae, 18*, 268–281.

Steiger, R. H., & Jäger, E. (1977). Subcommission on geochronology: Convention on the use of decay constants in geo- and cosmochronology. *Earth and Planetary Science Letters, 36*, 359–362